Postprint of: Dorozhovets M., Pawłowski E., Świsulski D., Frequency measurement research with weight averaging of pulse output signal of voltage-to-frequency converter, MEASUREMENT, Vol. 216 (2023), 112912, DOI: 10.1016/j.measurement.2023.112912

Frequency measurement research with weight averaging of pulse output signal of voltage-to-frequency converter

M. Dorozhovets[1,2)], E. Pawłowski[3], D. Świsulski[4)]

[1)]Department of Metrology and Diagnostic Systems, Faculty of Electrical and Computer Engineering, Rzeszow University of Technology, ul. Wincentego Pola 2A, 35-959, Rzeszów, Poland, michdor@prz.edu.pl
[2)]Department of Information and Measuring Technology, National University Lviv Polytechnic, Lviv, Ukraine
[3)]Faculty of Electrical Engineering and Computer Science, Lublin University of Technology, Lublin, Poland
[4)]Faculty of Electrical and Control Engineering, Gdansk University of Technology, Gdansk, Poland

Abstract. The paper presents the essence and investigation of the efficiency of weight averaging of a pulse output signal of voltage-to-frequency converter. The effect of sampling errors and the interference in the input signal during voltage-to-frequency conversion on the result of weight averaging is analyzed. A general form of the dependence of the averaging result on the signal value, interference level and the used weight function is derived. It is shown that from the point of view of sampling error reduction, the best are polynomial weight functions. In the case of high interferences whose frequencies are unstable or may change over a wide range, the specified level of their suppression, together with the reduction of the sampling effect, can be achieved using weight functions, such as trigonometric, with an appropriate level of side lobes. The level of interference suppression both in the narrow and wide frequency ranges, as well as the sampling error when using selected weight functions, have been tested by both simulation and experimentally. The obtained results show very good convergence with the values calculated from theoretical formulas.

Key words: Measurement; Pulse frequency; Interference; Counting effect; Weight function; Windows; NMRR.

1. Introduction

A frequency-modulated impulse signal is widely used in measuring systems due to its simple conversion and high immunity to the noise and interferences occurring in transmission channels. Voltage-to-Frequency Converters (VFC) are easily available because they are produced in the form of integrated circuits by many electronic companies [1 - 7]. Such converters are widely used due to their low price and, what is very important, due to high metrological parameters [1 - 7].

Various aspects concerning the construction, technology and application of such converters and the processing of frequency-modulated signals are presented in a number of publications [8 – 19]. Often VFC must meet specific requirements, such as low input voltages, very low consumption, etc. In [8] a circuit for a bipolar differential voltage-to-frequency converter is described. The system was implemented using Zetex transistor array circuits. In [9] a clock-controlled voltage-to-frequency converter is presented, in which the output frequency is proportional to the square root of the input voltage. Accuracy of approximately 0.02% of full scale for the 1 mV to 10 V input voltage range was achieved using commercially available CMOS components. A paper [10] presents an innovative thermal flow sensor with a frequency output. The sensor generates a series of output pulses whose frequency depends on the rate of fluid flow around the self-heating thermistor. The article [11] presents the problem of using multi-channel measuring systems of sensors converting the input value to the frequency of the impulse signal. Algorithms for digital processing of pulse frequency signals in offline and online modes are presented, which allow the acquisition of samples in selected regularly spaced moments of time.

In [12] the VFC that designed and implemented in 130 nm CMOS technology is proposed. The presented VFC can be used in complex ultra-low-voltage systems for the input range of 0 – 10 mV. In [13] a VFC designed using unipolar metal-oxide thin film transistor is proposes. This VFC can be used in flexible low-voltage sensor interfaces. Some fabricated aspects and also metrological parameters of the current-to-voltage-to-frequency converting current transducer, which can be effectively applied to bio-sensing devices requiring a compact area and low power consumption are presented in [14]. In [15] the sensor prototype for volt-second sensing based on the concept of an analog synchronous voltage-to-frequency converter, which can be used to built measuring technique for precise volt-second sensing that

combines the advantages of analog circuit technology with the performance of an FPGA, is presented and working principle is demonstrated by simulations and validated by measurements.

VFC can also be used in measuring systems with non-electrical sensors. For example a system of high-accuracy temperature measurement based on thermistor and voltage-to-frequency converter is designed and analyzed in [16].

In [17] presented the construction and experimental results of a power supply of range 0 - 5 volts which is further supplied to a voltage to frequency converter circuit built on 555-analog timer. The VFC can be used also to build the power supply for AC loads. For example, in [18] a new VFC that converts both voltage and frequency to the required level of voltage and frequency in low voltage networks used as a universal power supply for sensitive AC loads, is presented and describes in detail.

VFC can also be used in so called insulation amplifiers, in which input and output parts are electrically separated. For this purpose often the voltage-to-frequency to transmit the analog signals as frequency form through the digital optical fiber is used. Namely, in [19] the design of the hardware and the parameters of the circuit structure based on the AD650 chip are analyzed and discussed in detail and experimental results are given.

In this paper, the impact of periodic interferences occurring during the integration of the input voltage in VFC is analyzed, along with the examination of the use of weight averaging (windowing) of the output impulse signal to ensure that the required resolution of frequency measurement is preserved and the impact of the abovementioned interferences reduced.

When processing the frequency-pulse modulated output signal, two important features must be ensured:

1) the desired limit of the maximum relative pulse counting error, and

2) the desired reduction level of the interferences existing in the signal during the frequency-pulse modulation.

If the usual measurement method is used, then the number of counted pulses is:

$$N_x = floor(f_x \cdot T), \tag{1}$$

where T is the pulse counting time. The two above features are ensured by assigning an appropriate counting time T. Usually, if the maximum counting error is $\delta_{c,max}$ and the approximate value of the measured frequency is f_x, then the minimum counting time should meet the condition:

$$T \geq \frac{1}{f_x \delta_{c,\max}}. \tag{2}$$

For example, if $\delta_{c,max}$= 0.01 % then the minimum number of counted pulses is $N_x = 10^4$, and at f_x = 10 kHz (often it is the highest precision range of VFC) the minimum counting time is T = 1 s, which is too much for frequency measurement. Reducing the time will immediately reduce the number of counted pulses and increase the counting error accordingly.

If the measured input signal is distorted by harmonic interference:

$$u_n(t) = U_m \cos(2\pi f_n t + \varphi), \tag{3}$$

where U_m, f_n, and φ are the amplitude, frequency, and initial phase of interference, respectively, then to reduce the effect of such interference, usually as minimum one or more (m) interference periods T_n are used to count the input pulses:

$$T = m \cdot T_n = \frac{m}{f_n}. \tag{4}$$

For example, if the interference caused by a power supply with frequency close to the nominal 50 Hz (60 Hz in North America), then the pulse count time is a multiple of 20 ms (16.667 ms in North America). This simple method is effective for a known and stable interference frequency. If the interference

frequency deviates from the nominal value by a relative value δ_f, then the suppression factor (NMRR – normal mode rejection ratio) of such interference is:

$$NMRR = 20 \cdot \lg\left[\frac{U_m}{|\Delta|_{\max}(U_m)}\right], \tag{5}$$

where $|\Delta|_{\max}(U_m)$ is the maximal absolute value of the error caused by the interference of amplitude U_m, is about $NMRR \approx -20\lg(|\delta_f|)$.

Due to the European standard EN 50160 (1999) [20], the power frequency is the mean value measured over 10 s with maximal deviation $\delta_f = \pm$ 1% (49.5 - 50.5 Hz) for 99.5% of week, and - 6% ...+4% (47 - 52 Hz) for 100% of week. For example, if $\delta_f = 1\%$ (0.01), then the effect of the interference on the result of frequency measurement is about 1% of U_m (NMRR = 40 dB). That is, even if the amplitude of the interference is about 10% of the value of the information component U_x, then such interference may cause an error of about 0.1%.

At the interference amplitude of 100% of the information component U_x, this error can be about 1 %. With the deviation of interference frequency amounting to about -5%, the rejection coefficient decreases to NMRR ≈ 25.6 dB, i.e., the error can reach large values ≈ 5.24% of U_m. In power supply systems for aircraft and other mobile vehicles with nominal network frequency of 400 Hz, the frequency instability is even greater, namely the frequency tolerance is ± 5% [21], and the maximum deviation can be up to 360 Hz (-10%). In practice, the interference can often be caused by the operation of electronic equipment, where the frequency of signals can vary over a wide band.

The aim of this paper is to examine the application of weight averaging (windowing) of the output pulses of voltage-to-frequency converter to provide a given counting error and suppress periodical interference in a wide range of frequencies in the shortest possible measurement time interval.

2. The essence of weight averaging (windowing) of a pulse frequency modulated signal

In this Chapter, the voltage – to - frequency conversion (*U/f* conversion) based on integration of the input signal is analyzed. It is assumed that VFC is unipolar, i.e., the input signal is always positive: $u(t) > 0$. When U_R is the nominal range of VFC, then the input signal U_{in} with harmonic interference $u_n(t)$ (3) can vary in the range:

$$0 < u(t) = U_{in} + u_n(t) = U_{in} + U_m \cos(2\pi f_n t + \varphi) \le U_R. \tag{6}$$

When the input informative voltage U_x is positive, i.e., $0 \le U_x \le U_{Rx}$, where U_{Rx} is the range of the informative voltage, then, taking account of the interference amplitude U_m, the constant offset voltage U_0 in the input signal must be used to satisfy condition (6). Therefore, when the information input voltage takes two extreme values: U_x - 0 and $U_x = U_{Rx}$ two conditions should be met:

$$0 < U_0 - U_m \;\&\; U_{Rx} + U_0 + U_m \le U_R. \tag{7}$$

Therefore, the value of the offset voltage U_0 should comply the condition:

$$U_m < U_0 \le U_R - U_{Rx} - U_m. \tag{8}$$

When the input informative voltage U_x is bipolar, i.e., $-U_{Rx} \le U_x \le U_{Rx}$, then for two extreme values: $U_x = -U_{Rx}$ and $U_x = U_{Rx}$ the value U_0 of constant offset voltage should comply the condition:

$$U_{Rx} + U_m < U_0 \le U_R - U_{Rx} - U_m. \tag{9}$$

If the interference amplitude U_m does not exceed, approximately, 100 % of the range of informative voltage U_{Rx}: $0 < U_m \le U_{Rx}$, then the value of U_0 can be assumed as function of U_{Rx}: $U_0 = \alpha \cdot U_{Rx}$, where, from (8) and (9), $\alpha > 1$ for positive input voltage and $\alpha > 2$ for bipolar input voltage. When the sensitivity of VFC is $S_f = f_R / U_R$, where f_R is the frequency range, then, at the absence of both the information voltage ($U_x = 0$) and the interference ($U_m = 0$), the output frequency f_0 and period T_0 depend on U_0:

$$f_0 = S_f U_0 = S_f \alpha \cdot U_{Rx}, \quad T_0 = \frac{1}{f_0} = \frac{1}{S_f \alpha \cdot U_{Rx}}. \tag{10}$$

In the frequency measurement time interval T, the number N_0 of pulses at VFC output is $N_0 = f_0 \cdot T$. However, in the presence of the informative voltage ($U_x \neq 0$) and the absence of interference ($U_m = 0$) the frequency $f_{x,0}$, period $T_{x,0}$, and number of pulses $N_{x,0}$ are equal, respectively, to:

$$f_{x,0} = f_0 \cdot \left(1 + \frac{U_x}{U_0}\right), \; T_{x,0} = T_0 \frac{U_0}{U_0 + U_x}, \; N_{x,0} = N_0 \cdot \left(1 + \frac{U_x}{U_0}\right). \tag{11}$$

At the presence of an interference, even with the constant informative voltage U_x, the output pulses are not regularly distributed over time. The modulation of their positions depends on the amplitude and frequency of the interference. The times t_i and t_{i-1} of successive pulses are determined from non-linear equations:

$$\int_{t_{i-1}}^{t_i} u(t)dt = \int_{t_{i-1}}^{t_i} \left(U_0 + U_x + U_m \cos(2\pi f_n t + \varphi)\right)dt = U_0 \cdot T_0, \; i = 1,..,N_x. \tag{12}$$

The maximum influence of harmonic interference on the result of processing occurs at the initial phase φ=0 in relation to the middle of the time interval T. Conversely, when the initial phase (for cosine) will be $\varphi = \pm\pi/2$ (i.e., sine model), the effect of interference will be equal to zero. Therefore, for the next analysis steps, the cosine model of interference has been assumed: $U_m \cos(2\pi f_n t)$.

To ensure a given suppression level of the interference with frequency varying in a wide range, weight averaging (windowing) [22] can be used:

$$M_x = \int_{-T/2}^{T/2} u(t) \cdot g(t)dt, \tag{13}$$

where M_x is the result of weight averaging (windowing), and $g(t)$ is the so-called weight function or window [23], which is symmetrical around the middle ($t = 0$) of the time interval T. The essence of weight averaging of the frequency modulated signal is based on the representation of the integral of the product of two functions (13), by the Stieltjes integral [24], with its further approximation by a sum [24]. Using the Stieltjes representation of the integral (13) gives:

$$M_x = \int_{-T_{wf}/2}^{T_{wf}/2} u(t) \cdot g(t)dt = \int_{-T_{wf}/2}^{T_{wf}/2} g(t)d\int_{-T_{wf}/2}^{t} u(\tau)d\tau = \int_{-T_{wf}/2}^{T_{wf}/2} g(t)dy(t) \approx \sum_{i=1}^{N_x} g(t_i)\Delta y(t_i), \tag{14}$$

where:

$$\Delta y(t_i) = y(t_i) - y(t_{i-1}) = \int_{t_{i-1}}^{t_i} u(\tau)d\tau \tag{15}$$

is the integral increment. If this increment is constant in (15): $\Delta y(t_i) = \Delta y = C_0 = const$, then the result of averaging in (14) is:

$$M_x \approx C_0 \sum_{i=1}^{N_x} g(t_i) = C_0 \sum_{i=1}^{N_x} g_i, \tag{16}$$

where N_x is the number of VFC output pulses over the duration of the weight function T_{wf}.

Therefore, according to (16), the result of signal weight averaging is the sum of samples g_i of the weight function (window), taken at times t_i of the appearance of pulses at VFC output. The essence of signal weight averaging is shown in Fig. 1.

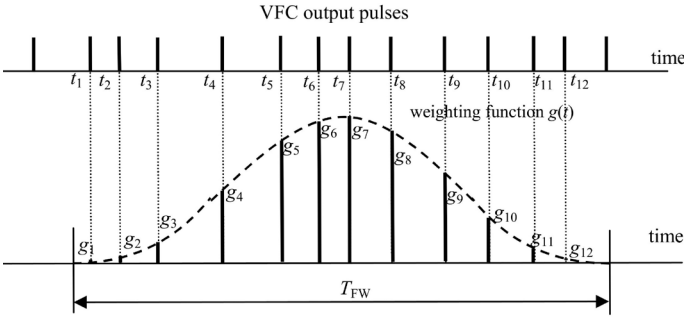

Fig. 1. The essence of averaging the frequency at VFC output.

If the function (window) $g(t)$ is normalized, i.e., $\int_{-T_{wf}/2}^{T_{wf}/2} g(t)dt = 1$ and when the input voltage is U_0 and output frequency is f_0 (10), then the sampling $g(t)$ (with sampling period $T_s = T_0$ (10)) gives $\int_{-T/2}^{T/2} g(t)dt \approx \sum_{i=1}^{N_0} g_i T_0 = \frac{1}{f_0}\sum_{i=1}^{N_0} g_i \approx 1$. From this we obtain:

$$\sum_{i=1}^{N_0} g_i \approx f_0 . \tag{17}$$

It follows from (17) that the frequency f_0 measured by the weight averaging method is equal to the sum of samples g_i of the weight function (window) $g(t)$ taken at times t_i of the appearance of pulses at VFC output. For an arbitrary value of the informative voltage U_x (input voltage U_0+U_x) determined by the weight averaging method, the informative frequency is equal to:

$$f_{Mx} \approx \sum_{i=1}^{N_x} g_i - f_0 . \tag{18}$$

The approximations in (17) and (18) depend on the used function (window) $g(t)$, the number N_x, and the irregularity of pulses at VFC output.

3. Dependence of the result of weight averaging of the pulse frequency modulated signal at VFC output

3.1 Mathematical model of pulse frequency modulated signal

As can be seen from Fig. 1 and from (12) - (18), to analyze the effectiveness of weight averaging it is necessary to know an explicit dependence of times t_i of the appearance of successive impulses at VFC output on the values of the input voltage (U_0+U_x) and the interference $u_n(t)$. This can be presented as the modulation of a sequence of non-modulated pulses of the offset U_0, the input informative U_x voltages (U_0+U_x), and the interference ($u_n(t)$) within the period T_0 (10). This modulation takes the form of the time shift $\tau(t)$ of the next pulse to time t [22] (Fig. 2). The time shift $\tau(t)$ is not constant because it depends on the value of variable interference $u_n(t)$. The value of $\tau(t)$ can be determined from the relationship (Fig. 2):

$$\int_{-T/2}^{t-\tau(t)} U_0 dt = \int_{-T/2}^{t} \left(U_0 + U_x + U_m \cos(2\pi f t)\right)dt . \tag{19}$$

Solving (19) gives:

$$t-\tau(t)=\frac{(U_0+U_x)(t+T/2)+(U_m/\omega)(\sin(\omega t)+\sin(\omega T/2))}{U_0}-\frac{T}{2}. \tag{20}$$

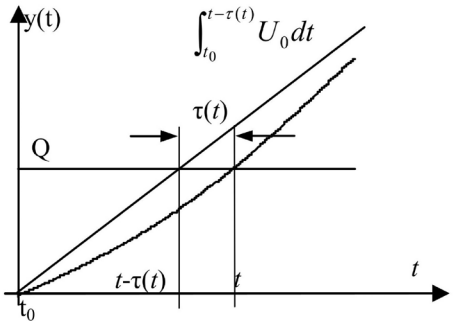

Fig. 2: Pulse shift $\tau(t)$ of information signal ($U_x < 0$) and interference $u_n(t) \neq 0$; $t_0 = -T/2$, Q is constant.

It is known from [25] that if the shift $\tau(t)$ of the δ-pulse varies, then the sequence of δ-modulated pulses can be described by:

$$u_{\delta M}(t)=\sum_{i=-\infty}^{\infty}\delta(t-\tau(t))=\frac{1}{T_0}\sum_{k-\infty}^{\infty}\frac{d[t-\tau(t)]}{dt}\cos\left(\frac{2\pi k}{T_0}(t-\tau(t))\right). \tag{21}$$

Since:

$$\frac{d[t-\tau(t)]}{dt}=\frac{U_0+U_x+U_m\cos(\omega t)}{U_0}, \tag{22}$$

then the frequency modulated pulse sequence given by (21) takes the form:

$$\begin{aligned}u_{\delta M}(t)=&\frac{C_0}{T_0U_0}(U_0+U_x+U_m\cos(\omega t))+\frac{2C_0}{T_0U_0}[U_0+U_x+U_m\cos(\omega t)]\times\\&\times\sum_{k=1}^{\infty}\cos\left(\frac{2\pi k}{T_0}\cdot\frac{U_0+U_x}{U_0}\cdot t+\frac{2\pi k}{T_0\omega}\cdot\frac{U_m}{U_0}\sin(\omega t)+\frac{\pi kT}{T_0}\cdot\frac{U_x}{U_0}+\frac{2\pi k}{T_0\omega}\cdot\frac{U_m}{U_0}\sin\left(\frac{\omega T}{2}\right)\right).\end{aligned} \tag{23}$$

Assuming $C_0/T_0U_0=1$ when the interference is absent (U_m=0) in (23), the relation is obtained for the sequence of δ-pulses with a fixed period (11) $T_{x,0}=T_0\cdot\frac{U_0}{U_0+U_x}$:

$$u_{\delta M,0}(t)=U_0+U_x+2(U_0+U_x)\sum_{k=1}^{\infty}\cos\left(\frac{2\pi k}{T_0}\cdot\frac{U_0+U_x}{U_0}\cdot t+\frac{\pi kT}{T_0}\cdot\frac{U_x}{U_0}\right). \tag{24}$$

3.2 Weight averaging of the frequency modulated signal

Let us use a normalized frequency $v=f\cdot T$. Then (23) takes the form:

$$\begin{aligned}u_{\delta M}(t)=&U_0+U_x+U_m\cos\left(2\pi v\frac{t}{T}\right)+2\left[U_0+U_x+U_m\cos\left(2\pi v\frac{t}{T}\right)\right]\times\\&\times\sum_{k=1}^{\infty}\cos\left[2\pi kn_0\frac{U_0+U_x}{U_0}\cdot\frac{t}{T}+\frac{kn_0}{v}\frac{U_m}{U_0}\sin\left(2\pi v\frac{t}{T}\right)+\pi kn_0\left(\frac{U_x}{U_0}+\frac{U_m}{U_0}\frac{\sin(\pi v)}{\pi v}\right)\right].\end{aligned} \tag{25}$$

The cosine in the sum component in (25) can be presented as a series using the first order Bessel functions $J_i(x)$ [24]:

$$u_{\delta M}(t) = U_0 + U_x + U_m \cos\left(2\pi v \frac{t}{T}\right) + 2\left[U_0 + U_x + U_m \cos\left(2\pi v \frac{t}{T}\right)\right] \times \\ \times \sum_{k=1}^{\infty} \sum_{i=-\infty}^{\infty} J_i\left(\frac{kN_0}{v}\frac{U_m}{U_0}\right) \cos\left[2\pi\left(kN_0\left(\frac{U_0+U_x}{U_0}\right) + i\cdot v\right)\cdot\frac{t}{T} + \pi k N_0\left(\frac{U_x}{U_0} + \frac{U_m}{U_0}\frac{\sin(\pi v)}{\pi v}\right)\right]. \tag{26}$$

Weight averaging of (26) gives:

$$M_x = \int_{-T/2}^{T/2} u_{\delta M}(t) g(t) dt = U_0 + U_x + U_m G(v) + \\ + 2\sum_{k=1}^{\infty} \cos\left(\pi k n_0\left(\frac{U_x}{U_0} + \frac{U_m}{U_0}\frac{\sin(\pi v)}{\pi v}\right)\right) \sum_{i=-\infty}^{\infty} J_i\left(\frac{kN_0}{v}\frac{U_m}{U_0}\right)\left\{(U_0+U_x) G\left(kN_0\left(\frac{U_0+U_x}{U_0}\right) + i\cdot v\right)\right. \\ \left. + \frac{U_m}{2}\left(G\left(kN_0\left(\frac{U_0+U_x}{U_0}\right) + (i+1)\cdot v\right) + G\left(kN_0\left(\frac{U_0+U_x}{U_0}\right) + (i-1)\cdot v\right)\right)\right\}, \tag{27}$$

where:

$$G(v) = \int_{-T/2}^{T/2} g(t) \cos\left(2\pi v \frac{t}{T}\right) dt \tag{28}$$

is the spectral characteristic (Fourier transformation) of the weight function.

For the Bessel function, the relation $J_{l-1}(x) + J_{l+1}(x) = \frac{2l}{x} J_l(x)$ is fulfilled [24], hence the last part of (27) can be regrouped to the form:

$$M_x = U_0 + U_x + U_m G(v) + 2\sum_{k=1}^{\infty} \cos\left(\pi k n_0\left(\frac{U_x}{U_0} + \frac{U_m}{U_0}\frac{\sin(\pi v)}{\pi v}\right)\right) \times \\ \times \sum_{i=-\infty}^{\infty} J_i\left(\frac{kN_0}{v}\frac{U_m}{U_0}\right)\left(U_0 + U_x + \frac{vU_0}{kN_0}\right) G\left(kN_0\left(\frac{U_0+U_x}{U_0}\right) + i\cdot v\right) \tag{29}$$

The values of the Bessel function for indexes larger than the values of the arguments disappear very quickly: i.e., at $i > x$ $J_i(|x|) \to 0$ [24] (Fig. 3). For example, at x= 20 and for $|i|$>25 $J_i(|x|) < 0.01$, and when x= 50, this condition is already met for i > 57. Therefore, by selecting the factor $\beta \cong 1.1..1.25$, which takes into account the disappearance of the function $J_i(|x|)$ (the higher the value of x, the closer the value of β to 1), we define the condition for index numbers (i) for which the values of the Bessel function are negligibly small:

$$|i| > i_0 \approx \beta \cdot x = \beta \frac{kN_0}{v}\frac{U_m}{U_0}. \tag{30}$$

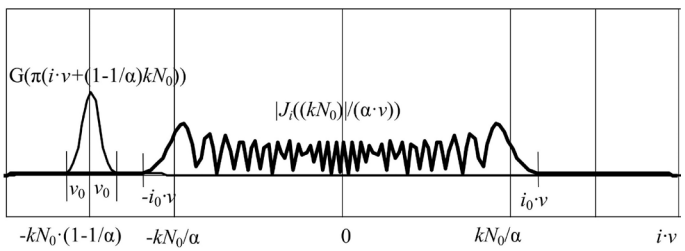

Fig. 3. Weight averaging properties of the frequency modulated signal.

The condition for suppressing the interference is that the interference frequency of harmonic components caused by the modulation does not reach the width $\pm v_0$ of the main lobe $G(v)$ (28). Therefore, the parameters of the frequency modulator should be chosen in such a way that the amplitudes of harmonic components (determined by the level of the function $J_i(|x|)$) do not overlap in the worst case with the width of the main lobe of the weight function spectral characteristic (Fig. 3). If the value of the main lobe of the weight function transformation G(v) is v_0, then, to meet the above condition, the influence of the harmonic components caused by the interference modulation should be below the set level (Fig. 3):

$$\left| kN_0\left(\frac{U_0+U_x}{U_0}\right)+i\cdot v\right| > v_0 . \tag{31}$$

The worst case of modulation takes place when $U_x = -U_{Rx}$ and $U_m = U_{Rx}$ (the lowest frequency of output pulses and the highest interference impact). Then $\frac{U_0+U_x}{U_0} \to 1-\frac{U_{Rx}}{U_0} = 1-\frac{1}{\alpha}$, and $\frac{U_m}{U_0} \to \frac{U_{Rx}}{U_0} = \frac{1}{\alpha}$. When including (29), the condition (31) for negative index values, can be given as:

$$kN_0\left(1-\frac{1}{\alpha}\right)-\beta\frac{kN_0}{\alpha} > v_0 \text{ , or } \quad 1-\frac{1+\beta}{\alpha} > \frac{v_0}{kN_0} . \tag{32}$$

With positive $k \geq 1$ and N_0>>1 in (31), we obtain the required value of α, which determines the value of the constant offset voltage U_0:

$$\alpha = \frac{U_0}{U_{Rx}} > \frac{1+\beta}{1-\frac{v_0}{kN_0}} \approx 1+\beta . \tag{33}$$

If $\beta \cong 1.25$, then for extreme values: $|U_x| \leq U_{Rx}$ and $U_m = U_{Rx}$, correct operation of the VFC (with the possibility of further interference suppression with the weight averaging method) requires meeting the condition $\alpha > \approx 2.25$ for the bipolar input signal. For the unipolar positive input voltage ($U_x \geq 0$), this condition is slightly different:

$$\alpha > \frac{\beta}{1-\frac{v_0}{kN_0}} \approx \beta \approx 1.25. \tag{34}$$

In general, when the interference is integrated, its amplitude decreases in proportion to the frequency f: $U_m/(2\pi fT) = U_m/(2\pi v)$. When $v \geq v_0$ and v_0=1 (uniform window) the interference influence decreases at least 2π times. With weight averaging, $v_0 \geq 2$ is usually applied, therefore the influence of the interference decreases at least 4π times. Therefore, the conditions (33) and (34) may be slightly less restrictive. However, for an arbitrary initial phase of the interference with the minimum signal value $U_{x,min}$ and the maximum amplitude of the interference $U_{m,max}$, the inequalities $U_0 + U_{x,\min} - U_{m,\max} \geq 0$ or $U_x = -U_{Rx}$, $U_{m,max} = U_{Rx}$ should always be met, which means meeting the condition $U_0 \geq 2U_{Rx}$ or $\alpha \geq 2$.

4. Effectiveness analysis of the frequency modulated signal weight averaging

4.1 The impact of the weight function (window) shape on the maximum pulse count error

The use of weight averaging provides two important advantages: it reduces the impact of the weight function sampling effect (i.e., pulse counting caused quantization of the result) and ensures the desirable level of suppressing interfering components in the given frequency band. These two important features of weight averaging depend on the shape and durability of the weight function. Therefore, there are two main

criteria for selecting the weight function (window). The 1st one refer to ensuring that the used weight function can reduce the counting effect to a given level, the 2nd concerns the ensuring that the used weight function can suppress of the interference components in the given frequency band to a given level.

As a result of sampling the weight function with period T_s=T_x, the area under the weight function is approximated, even if the integer numbers N_x of the sampling period T_s=T_x fall exactly in the durability of the weight function T, i.e., $N_x T_x = T$. It is known [24] that when using the trapezoidal method for integration, the maximum error of function area determination is given as:

$$\Delta_{1,s} \le \frac{T_x^3}{12}\left|g''(t)\right|_{\max} = \frac{T^3}{12N_x^3}\left|g''(t)\right|_{\max}, \tag{35}$$

where $g''(t)$ is the second order derivative of the weight function.

The second component, which is also related to sampling, is caused by the lack of sampling synchronization with the durability of the weight function, i.e., $N_x T_x \neq T$. If the beginning of the weight function formation is synchronized with the next pulse from the modulator output, then the maximum difference $T - N_x T_x$ must not exceed the value $T_x \approx T/N_x$, i.e.

$$\left(T - N_x T_x\right)_{\max} < T_x . \tag{36}$$

Then the maximum error in determining the surface under the weight function is:

$$\Delta_{2,s} < \int_{T/2-T/N_x}^{T/2} g(t)dt . \tag{37}$$

When $N_x >> 1$, the application of the trapezoidal method to (37) gives:

$$\Delta_{2,s} < \int_{T/2-T/N_x}^{T/2} g(t)dt \approx \frac{1}{2}\cdot\frac{T}{N_x}\left[g\left(\frac{T}{2}\left(1-\frac{2}{N_x}\right)\right)+g\left(\frac{T}{2}\right)\right]. \tag{38}$$

Since the surface under the normalized weighting function (window) is equal to 1 ($s_g = \int_{-T/2}^{T/2} g(t) = 1$), the error values given by (35) and (38), and also the relative errors (in relation to the surface under the weight function), are:

$$\delta_{1,s} = \frac{\Delta_{1,s}}{s_g} = \Delta_{1,s}, \quad \delta_{2,s} = \frac{\Delta_{2,s}}{s_g} = \Delta_{2,s} . \tag{39}$$

The absolute error values (in hertz) are equal to:

$$\Delta_{1,f} = \delta_{1,s}\cdot f_x = \frac{\delta_{1,s}\cdot N_x}{T}, \quad \Delta_{2,f} = \delta_{2,s}\cdot f_x = \frac{\delta_{2,s}\cdot N_x}{T}. \tag{40}$$

On the other hand, the error values normalized to the nominal range $f_R = S_f U_R$ of the informative frequency component are equal to:

$$\delta_{1,f_n} = \frac{\Delta_{1,f}}{f_R} = \frac{\delta_{1,s}\cdot N_x}{N_R}, \delta_{2,f_n} = \frac{\Delta_{2,f}}{f_R} = \frac{\delta_{2,s}\cdot N_x}{N_R}. \tag{41}$$

where $N_R = f_R \cdot T$ is the nominal number of pulses (range) corresponding to the nominal informative range f_R of the frequency component.

Uniform (rectangular) weight function (window). If there is the requirement to reduce only the sampling effect, the simplest conventional counting, i.e., the uniform (rectangular) weight function (window) is used:

$$g_U(t) = \frac{1}{T}\begin{cases}1, if\ |t| \le T/2,\\ 0, \text{otherwise.}\end{cases} \tag{42}$$

For this function $g''(t) = 0$, and therefore the error component (34) is equal to zero: $\Delta_{1,s,U} = 0$, while the second component in (39) takes the well-known value:

$$\delta_{2,s,U} \approx \frac{1}{N_x}. \tag{43}$$

According to (40), it follows from (43) that the relative and absolute errors caused by sampling are:

$$\delta_{2,f_n,U} \approx \frac{100\%}{N_x},\ \ \Delta_{2,U} \approx \frac{1}{T}, \text{Hz}. \tag{44}$$

Triangular weight function (window). The triangular weight function (window) is described by:

$$g_T(t) = \frac{2}{T}\begin{cases}1 - 2|t|/T,\ |t| \le T/2,\\ 0, \qquad \text{otherwise.}\end{cases} \tag{45}$$

For this function $g''(t) = 0$, and therefore the error component (35) is also equal to zero: $\Delta_{1,s,T} = 0$. For the triangular window the second component in (38) is:

$$\delta_{2,s,T} = \frac{2}{N_x^2}. \tag{46}$$

According to (40), it follows from (46) that the relative and absolute errors caused by sampling are:

$$\delta_{2,f_n,T} \approx \frac{200\%}{N_x^2}.\ \ \Delta_{2,T} \approx \frac{2}{N_x \cdot T}, \text{Hz}. \tag{47}$$

For example, if N_x=100, then the maximum relative counting error for conventional measurement (i.e., using the uniform window) is 1% and for the triangular function this error is only 0.02%. If $N_x = 1000$, the maximum relative counting error for conventional frequency measurement is 0.1%, and for the triangular function it is essentially lover: 0.0002%. As we can see, the effectiveness of the triangular function is very significant.

4.2. Choosing the weight function that provides the desired level of interference suppression

Unfortunately, due to the presence of variable-frequency interference in the VFC input, the distribution of time positions of successive pulses after modulation is significantly irregular and therefore the use of a triangular or parabolic function will not provide the desired level of interference suppression when its frequency is not stable and may change in a wide range. For this purpose, it is necessary to use other functions (windows) that provide the most important averaging parameters: the specified level of suppression (NMRR) of the harmonic components, and the smallest possible width of the main lobe (v_0) of the spectral characteristic that determines the time interval of averaging at the specified minimum frequency (f_{low}) of interference: $T_{av} = T = v_0/f_{low}$. In addition, these functions should provide the specified minimum sampling error and should be easily calculated online when the next pulse arrives.

From the calculation point of view, the simplest weight functions are trigonometric functions, e.g., those proposed by Hamming, Blackman, Harris, and others [23]. It is worth noting here that the direct use of the optimal (in terms of the width of the main lobe v0) Dolph - Chebyshev function (window) [23] causes a problem, related to the fact that this function is discrete, i.e., not continuous, and its use requires interpolation, which leads to additional inaccuracies.. The parametric Kaiser function (window) [23],

whose parameters can be changed depending on the averaging parameters specified, requires calculating the modified Bessel function when the new pulse arrives, which results in additional calculation efforts.

The application of several trigonometric weight functions will be analyzed below from the point of view of effectiveness of frequency modulated pulse weight averaging. In these analyses, normalized weight functions will be used for which the surface area is equal to 1.

The **normalized Hamming weight function** (window) [23], which is one of the simplest weight functions, is defined as:

$$g_H(t)=\frac{1}{T}\begin{cases}1+\dfrac{0.46}{0.54}\cos\left(2\pi\dfrac{t}{T}\right), & 0\le\dfrac{|t|}{T}\le\dfrac{1}{2},\\ 0, & \text{othewise}.\end{cases} \tag{48}$$

This function provides harmonic suppression (NMRR_H) of over 42 dB. In many cases, this suppression may be sufficient. The width of the main spectral lobe is v_0=2, i.e., for suppression of harmonic components starting from the frequency f_{low}, the time interval equal to a minimum of 2 interference periods T_{low} is needed: $T=T_H=2/f_{low}=2T_{low}$.

For this function, the relative sampling error is reduced linearly to N_x: ($2\pi/N_x<<1$):

$$\delta_{2,s,H}=\frac{1}{N_x}\left(1-\frac{0.46}{0.54}\cdot\frac{\sin(2\pi/N_x)}{2\pi/N_x}\right)\approx\frac{0.15}{N_x}. \tag{49}$$

According to (40), it follows from (49) that the relative and absolute errors caused by sampling are, respectively:

$$\delta_{2,f_n,H}\approx\frac{15\%}{N_x}.\quad\Delta_{2,H}\approx\frac{0.15}{T},\ \text{Hz}. \tag{50}$$

Considering the error values (49) caused by the sampling effect, the Hamming function is not sufficient to realize weight averaging of VFC output frequency pulses.

The **normalized Blackman weight function** (window) [23] is given as:

$$g_B(t)=\frac{1}{T}\begin{cases}1+1.1756\cos\left(2\pi\dfrac{t}{T}\right)+0.18772\cos\left(4\pi\dfrac{t}{T}\right), & 0\le\dfrac{|t|}{T}\le\dfrac{1}{2},\\ 0, & \textit{otherwise}.\end{cases} \tag{51}$$

This function provides harmonic suppression (NMRR_B) of over 70 dB. The width of the main lobe is v_0=3, i.e., for the suppression of harmonic components in the band starting from the lower frequency f_{low}, a minimum of 3 periods of interference is needed: $T=T_B=3/f_{low}$. For this function, the relative and absolute errors caused by sampling are about 13 times smaller compared to the value for the Hamming function, and about 90 times smaller compared to conventional pulse counting. The relative sampling error decreases with increasing N_x:

$$\delta_{2,s,B}\approx\frac{0.0116}{N_x}. \tag{52}$$

According to (41) and (52), when the Blackman function is used, the relative and absolute errors caused by sampling are equal to:

$$\delta_{2,f_n,B}\approx\frac{1.16}{N_x},\%.\quad\Delta_{2,f_n,B}\approx\frac{0.0116}{T},\ \text{Hz}. \tag{53}$$

The **normalized Blackman-Harris weight function** (window) [22]**.** There are several variants of this function. One of them, the four-component function is given by the normalized relationship:

$$g_{BH}(t)=\frac{1}{T}\begin{cases}1+1.36109\cos\left(2\pi\frac{t}{T}\right)+0.39381\cos\left(4\pi\frac{t}{T}\right)+0.03256\cos\left(6\pi\frac{t}{T}\right), & 0\le\frac{|t|}{T}\le\frac{1}{2},\\ 0, & \text{otherwise}.\end{cases} \quad (54)$$

This function provides harmonic suppression (NMRR_BH) of over 90 dB. The width of the main lobe is v_0=4, i.e., for suppression of harmonic components in the band starting from the lower frequency f_{low}, a minimum of 4 periods of interference is needed: $T = T_{BH} = 4/f_{low}$.

When using this function, the relative sampling error is significantly smaller than those for the previous functions, namely, at N_x>200 the asymptotic error value is:

$$\delta_{2,s,BH} \approx \frac{0.00017}{N_x}. \quad (55)$$

According to (41) and (55), when the Blackman-Harris function is used, the relative and absolute errors caused by sampling are equal to:

$$\delta_{2,f_n,BH} \approx \frac{0.017}{N_x},\%. \quad \Delta_{2,f_n,BH} \approx \frac{0.00017}{T}, \text{ Hz}. \quad (56)$$

We can see that the Blackman-Harris function provides high (90 dB) interference suppression and very small sampling error (56). However, the averaging durability is relatively high - 4 harmonic periods with the lowest frequency are needed.

Fig. 4 shows the dependence of relative (a) and absolute (b) errors on the number N_x of pulses for different weight functions. The averaging time is T=60 ms, the same as for the Blackman function.

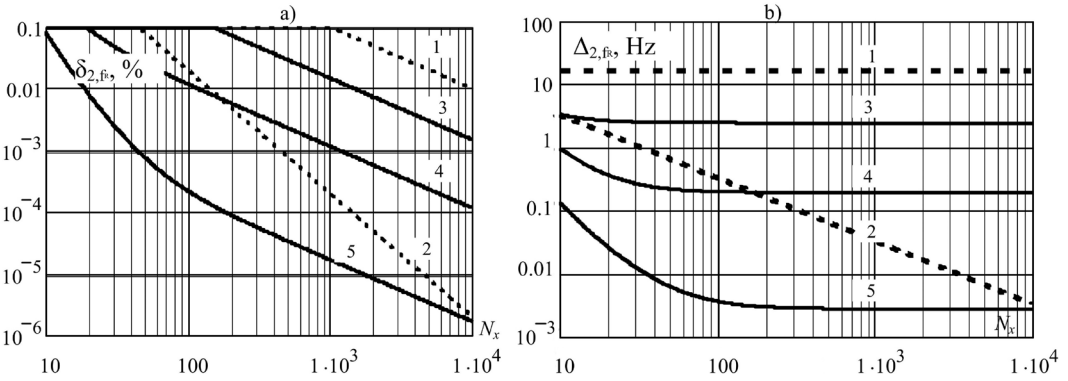

Fig 4. Normalized (to the range f_R of the frequency information component) errors for the number N_x of pulses: a) relative, b) absolute. Weight functions: 1 - rectangular, 2 - triangular, 3 - Hamming, 4 - Blackman, 5 - Blackman-Harris.

As shown in Fig. 4, with N_R > 100 the specified error level of 0.01% associated with sampling of the weight function can be achieved using the Blackman and Blackman-Harris weight functions as well as the triangular function. However, the triangular function does not provide a sufficient level of suppression of harmonic interference in the wide frequency range - the level of the spectral side lobe is about 27 dB.

When using the Blackman weight function, for which the weighting time equals 3 harmonic periods with the lowest frequency ($T_B = 3/f_{low}$), relatively good interference suppression is provided (NMRR_B=70 dB). When $N_x \ge 1000$ at the minimum value of the information signal ($U_x = -U_{Rx}$), the sampling error (53) is ≤ 0.00116%. Even when $N_x \ge 100$, the sampling error (53) is ≤ 0.0116%. Therefore, using the Blackman function is recommended when measuring the frequency with weight averaging.

4.3 Results of weight averaging tests

4.3.1. Study of the error caused by VFC pulse sampling of the weight function (window)

The parameters of the performed study were:

VFC: U_n=10 V, f_n =10 kHz, S_f=1 kHz/V. Averaging functions (windows): uniform (U), triangular (T), Blackman (B), Blackman-Harris (BH). Averaging times: 1) TU = 20 ms, TT = 40 ms, TB = 60 ms, TBH = 80 ms; 2) $TU = TT = TB = TBH = T_{av}$ = 80 ms.

Input unipolar voltages: U_{in1}= 4.551167 V, U_{in2}=4 .548833 V; output frequencies f_{x1}= 4.551167 kHz, f_{x2}= 4.548833 kHz; periods: T_{x1}= 0.19724 ms, T_{x2}= 0.19837 ms. For these values, the products $T_{av}{\cdot}f_{x1}$= 364.093, $T_{av}{\cdot}f_{x2}$= 363.907 are close to each other, but the total number of periods in the weight averaging duration differ by 1 (N_{x1}= 364, N_{x2}= 363), which results in averaging error values close to the maximal values.

In the simulation, each start of weight averaging is shifted by dT = 1 μs, giving T_x/dT = 220 times in total. The relative errors of weight averaging of frequency pulses obtained for the input voltages U_{in1}= 4.551167 V and U_{in2}= 4.548833 V are presented in Table 1. This Table also includes the theoretical values of these errors calculated from (44), (47), (53) and (56). Comparing the maximum weight averaging errors obtained from the simulations with those calculated theoretically, we can see that they are very close to each other.

Table 1. Maximal relative errors (δ_{Ux}, %) of weight averaging of frequency pulses obtained from simulation and theory.

Window	U_{in} =4.548833 V		U_{in} =4.551167 V	
	δ_{Ux}, simulation	δ_{Ux}, theoretical	δ_{Ux}, simulation	δ_{Ux}, theoretical
Uniform (20ms)	1.074 %	1.10%	1.073%	1.10 %
Triangular (40ms)	$0.268{\cdot}10^{-3}$%	$6.04{\cdot}10^{-3}$%	$0.262{\cdot}10^{-3}$%	$6.04{\cdot}10^{-3}$%
Blackman (60ms)	$3.95{\cdot}10^{-3}$%	$4.25{\cdot}10^{-3}$%	$3.94{\cdot}10^{-3}$%	$4.25{\cdot}10^{-3}$%
Blackman-Harris (80ms)	$4.16{\cdot}10^{-5}$%	$4.07{\cdot}10^{-5}$%	$4.17{\cdot}10^{-5}$%	$4.67{\cdot}10^{-5}$%
Uniform (80ms)	0.249 %	0.275%	0.249 %	0.275%
Triangular (80ms)	$1.31{\cdot}10^{-4}$%	$1.51{\cdot}10^{-3}$%	$1.28{\cdot}10^{-4}$%	$1.51{\cdot}10^{-3}$%
Blackman (80ms)	$2.88{\cdot}10^{-3}$%	$3.19{\cdot}10^{-3}$%	$2.88{\cdot}10^{-3}$%	$3.19{\cdot}10^{-3}$%

If, during the averaging, the total number of signal periods at VFC output changes very little from the duration of the weight function (window), then the maximum error will be very close to the maximum theoretical value for each window.

4.3.2. Study of periodic interference suppression by weight averaging

When studying the interference suppression, there are two basic error components to consider: the first is related to direct influence of the interference, and the second to the influence of the window sampling (weight function) analyzed above. Therefore, for each window, the normal mode rejection ratio (NMRR) depends not only on the frequency and initial phase of the interference but also on the sampling effect of the window.

The parameters of the study were: VFC: U_n=10 V, f_n = 10 kHz, S_f = 1 kHz/V. Input voltage U_{in1}= 4.551167 V, the same as above. Interference: amplitude U_m= 2.5 V, nominal frequency $f_{i.n}$= 50 Hz, nominal period T_n=1/$f_{i.n}$= 20 ms; frequencies: 48 Hz, 49 Hz, 49.5 Hz, 50 Hz, 50.5 Hz, 51 Hz, 52 Hz; phase shift: from 0 to 360° with 2° step. Averaging functions (windows): uniform (rectangular) (U), triangular (T), Blackman (B). Averaging time: $TU = T_n$= 20 ms. $TT = 2T_n$ = 40 ms, $TB = 3T_n$= 60 ms. The theoretical minimal values of NMRR in the interference frequency range from 48 to 52 Hz which were obtained using the uniform, triangular and Blackman weight functions (windows) are given in Table 2. From this Table we can find that the minimal theoretical values of NMRR are near the frequency limits 48 and 52 Hz.

In the presence of interference, the conversion of voltage into pulse frequency by (12) with further application of weight averaging causes nonlinear effects, which means that the NMRR does not depend solely on the value of the interference amplitude. Theoretically, at the interference frequency 50 Hz, the value of the NMRR goes to infinity (Tab. 2). However, due to the influence of the sampling effect of the weight function, as shown above in (44), (47), (53), and (56), the sampling errors are not equal to 0.

The variability of the frequency error Δ_{2,f_x}, converted into voltage: $|\Delta|_U = \Delta_{2,f_x} / S_f$ (V), and the NMRR has been analyzed for three interference amplitudes: 2.5 V, 0.25 V, and 0.025 V, in the frequency interference range from 48 Hz to 52 Hz. The results are given in Table 3.

Table 2. Theoretical values of NMRR in the frequency range 48 Hz – 52 Hz.

f, Hz	NMRR, dB		
	Uniform window	Triangular window	Blackman window
48	27.6	55.3	59.9
49	33.8	67.6	68.3
49.5	39.9	79.8	75.5
50	∞	∞	∞
50.5	40.1	80.2	78.2
51	34.2	68.3	73.7
52	28.3	56.6	70.9

Table 3. Frequency weight averaging errors converted into voltage $|\Delta|_U$ (mV) and NMRR values (dB) at interference amplitudes 2.5 V, 0.25 V, and 0.025 V.

f, Hz	Window	U_m=2.5 V		U_m=0.25 V		U_m=0.025 V	
		$\|\Delta\|_U$, mV	NMRR, dB	$\|\Delta\|_U$, mV	NMRR, dB	$\|\|\Delta\|_U$, mV	NMRR, dB
48	Uniform	101	27.9.	51.2	13.8	48.8	-5.8
	Triangular	4.33	55.2	0.433	55.2	0.043	55.3
	Blackman	2.51	60.0	0.341	57.3	0.193	42.2
49	Uniform	51.2	33.8	51.2	13.8	48.8	-5.8
	Triangular	1.04	67.6	0.12	66.4	0.017	63.5
	Blackman	0.97	68.2	0.244	60.2	0.183	42.7
49.5	Uniform	48.8	34.2	48.8	14.2	48.8	-5.8
	Triangular	0.329	77.6	0.034	77.3	0.0093	68.5
	Blackman	0.498	74.0	0.219	61,2	0.181	42.8
50	Uniform	48.8	34.2	48.8	14.2	48.8	-5.8
	Triangular	0.0091	108.7	0.012	86.2	0.012	66.3
	Blackman	0.179	82.9	0.179	62,8	0.179	42.9
50.5	Uniform	51.2	33.8	48.8	14.2	48.8	-5.8
	Triangular	0.328	77.6	0.025	80.0	0.0097	68.2
	Blackman	0.393	76.1	0.180	62,8	0.180	42.8
51	Uniform	51.2	33.8	48.8	14.2	48.8	-5.8
	Triangular	0.963	68.3	0.099	68.9	0.015	64.2
	Blackman	0.557	73.0	0.180	62.8	0.180	42.8
52	Uniform	101	27.8	48.8	14.2	48.8	-5.8
	Triangular	3.70	56.6	0.384	56.7	0.042	55.4
	Blackman	0.798	69.9	0.183	62.7	0.183	42.7

At the interference frequency of 50 Hz, the error is caused mainly by the sampling effect and is practically independent of the interference amplitude (Tab. 3). For the parameter values: U_{in1} = 4.551167 V, S_f = 1 kHz/V, TU = 20 ms, TT = 40 ms, TB = 60 ms, and in the absence of interference, the minimal values of the error $|\Delta|_{min}$ (mV), determined from (44), (47) and (53) and converted into voltage, are equal to: $\Delta_{U,U\_max} \approx$ 50 mV (uniform window), $\Delta_{U,T,max} \approx$ 0.012 mV (triangular window) and $\Delta_{U,B,max} \approx$ 0.18 mV (Blackman window). Therefore, at the interference frequency of 50 Hz, the errors of the averaged pulse values at VFC output for different interference amplitudes should practically be equal to these values Since the amplitude of the interference decreases sequentially by 10 times, therefore, the NMRR decreases by about 20 dB. Namely, at the amplitude of 0.025 V, the error caused by uniform window sampling is almost twice the amplitude, so the NMRR is negative and equal to about – 6 dB in this case. When the interference frequency deviates from 50 Hz, the effect of interference

amplitude is magnified compared to that of sampling, especially when using triangular and Blackman windows.

4.3.3. Study of NMRR in wide frequency range

Since the triangular window does not provide satisfactory interference suppression over a wide frequency band (Fig. 5), therefore, only interference suppression using the Blackman window was further analyzed.

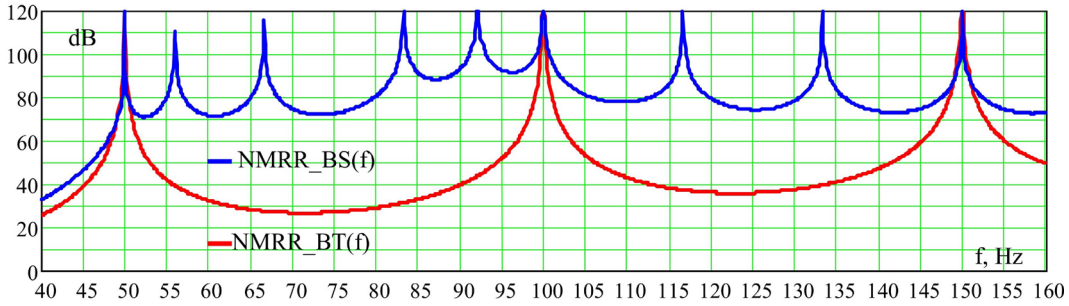

Fig. 5. Theoretical minimal NMRR values in wide frequency band 40 – 160 Hz (b), using Blackman (NMRR_B(f)) and triangular (NMRR_T(f)) windows.

The interference amplitude assumed in the simulation was $U_m = 2.5$ V. The following frequencies were selected from Fig. 6: 52.5 Hz, 61 Hz, 74.2 Hz, 110 Hz, 125 Hz, 141.7 Hz, 158.3 Hz, (with corresponding normalized frequencies $v = f \cdot T_n = 3.15, 3.66, 4.45, 6.6, 7.5, 8.5, 9.5$). For these frequencies, the NMRR_B(f) of the Blackman windows had the (minimal) levels of: 70.9 dB, 71.3 dB, 72.0 dB, 77.6 dB, 74.1 dB, 72.9 dB, 72.5 dB, respectively. When the normalized frequency was $v > 10$, then NMRR_B(f) tended to increase above 72 dB. The averaging time was: $TU = T_n = 20$ ms, $TT = 2T_n = 40$ ms, $TB = 3T_n = 60$ ms.

The results of NMRR_BS(f) obtained from the simulations are compared in Fig. 6 with the corresponding theoretical values NMRR_BT(f).

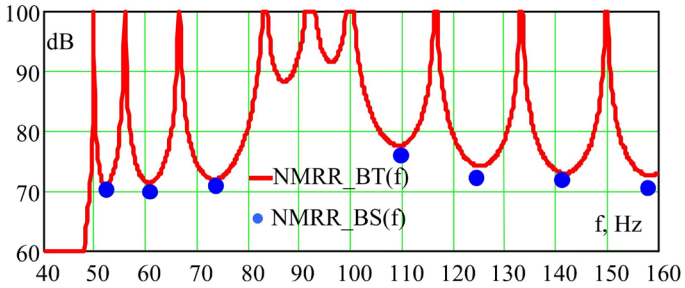

Fig. 6. Comparing NMRR_BS(f) values obtained from simulation with theoretical values NMRR_BT(f)

From Fig. 6 we can see that using the Blackman window for averaging pulses at VFC output when the input voltage is distorted by interference of any frequency above the minimum value $f_{\min} = f_{i,n}$, the obtained suppression (NMRR_B) of the influence of these interferences is close to the theoretical level.

4.3.4. Study of the influence of random deviations of times of appearance of VFC output pulses

An additional factor influencing the result of weight averaging is random deviations of the times of appearance of pulses at the VFC output. These deviations are caused by the external noise in the input signal and the internal noise of VFC chain elements. Since this effect occurs both in the presence and absence of regular interference, a decision was made to investigate it for the input signal without regular interference.

It was assumed that random deviations Δt_i of adjacent impulses are independent of each other, and have zero expected value and standard deviation σ_t. Then, as a result of the appearance of deviation Δt_i of *i*-pulse at time t_i, the value of the weight function is changed by:

$$\Delta g_i \approx g'(t_i) \cdot \Delta t_i, \tag{57}$$

where $g'(t_i)$ is the weight function derivative.

Assuming the independence between the random deviations, the sum of the values of the weight function (5) will have a random component with variance:

$$\sigma_g^2 \approx \sigma_t^2 \sum_{i=1}^{N_x} (g'(t_i))^2 . \tag{58}$$

From (58) we can see that the variance σ_g^2 depends on the sum of squares of the derivative weight function values. It can be easily shown that for the trigonometric weight functions considered above, this sum is proportional to the number of pulses:

$$\sum_{i=1}^{N_x} (g'(t_i))^2 \cong \frac{C_{g'}}{T^4} \cdot N_x . \tag{59}$$

where $C_{g'}$ is the constant depending on the coefficients of the used weight function. In particular, for the Blackman and Blackman-Harris functions, this constant is:

$$\begin{aligned} C_{g'B} &= \frac{(2\pi)^2}{2} \cdot \left(1.1756^2 + 4 \cdot 0.18772^2\right) \approx 30.06; \\ C_{g'BH} &= \frac{(2\pi)^2}{2} \cdot \left(1.36109^2 + 4 \cdot 0.39381^2 + 9 \cdot 0.03256\right) \approx 49.00 . \end{aligned} \tag{60}$$

Therefore, standard uncertainty caused by random deviations of the output pulses is:

$$u(f)_{\sigma_t} = \frac{\sigma_t}{T^2} \sqrt{C_{g'} \cdot N_x} . \tag{61}$$

In the absence of noise and regular interference, the number of output pulses in the weight function is $N_x = T \cdot f_x$, i.e. $f_x = N_x / T$. Hence, relative standard uncertainty caused by this effect is:

$$u_{rel}(f)_{\sigma_t} = \frac{\sigma_t}{T} \sqrt{\frac{C_{g'}}{N_x}} \cdot 100\% . \tag{62}$$

For example, when the Blackman weight function is used ($T = 60$ ms, $C_{g'B}$=30.06) for the VFC: U_n=10 V, f_n=10 kHz, S_f=1 kHz/V, and for the input voltage $U_x \approx U_n / 2 = 5$ V and output frequency $f_x \approx 5$ kHz, i.e., $N_x = f_x \cdot T = 300$, assuming that the standard deviation σ_t is about 1 μs (0.5 % of period T_o), the relative standard uncertainty from (62) is:

$$u_{rel}(f)_{\sigma_t} = \frac{1 \cdot 10^{-6}\,\mathrm{s}}{0.06\,\mathrm{s}} \sqrt{\frac{30.06}{300}} \cdot 100\% \approx 0.0005\,\%\,.$$

Comparing this value with that obtained from (53) $\delta_{2,s,B} \approx 1.16\% / N_x \approx 0.004\,\%$, we can see that the uncertainty component caused by random deviation of pulses is significantly smaller than the error obtained from (53): 0.004% at N_x=300. Even when the standard deviation σ_t is of about 2% of period T_x (σ_t=4 μs), the relative standard uncertainty (62) $u_{rel}(f)_{\sigma_t} \approx 0.002\,\%$ is still less than the error from (53). In other words, if the standard deviation of random variations in pulse timing is not more than a few percent of the pulse period, then its effect on the averaging result is relatively small.

5. Experiments

5.1. Test stand

In order to practically verify the results of theoretical analysis and simulations, a suitable test stand was built and a series of experiments were carried out to process and analyze the output signal of the actual voltage to frequency converter (VFC). Fig. 7 shows a block diagram of the measurement system used. The implemented VFC converter was based on LM331 IC, in accordance with the application circuit recommended by the manufacturer [26]. The LM331 converter converts negative voltage in the range of – 10 V ... 0 V to the frequency:

$$f_x(t) = \begin{cases} 0, & u_x(t) \geq 0, \\ S_f \cdot u_x(t), & -10\ \mathrm{V} \leq u_x(t) < 0. \end{cases}, \tag{63}$$

where: $f_x(t)$ is the converter output frequency, $u_x(t)$ is the test input voltage of the converter, and S_f is the sensitivity of the converter. Note that the sensitivity of the LM331 converter has a negative value: S_f = – 1 kHz / V.

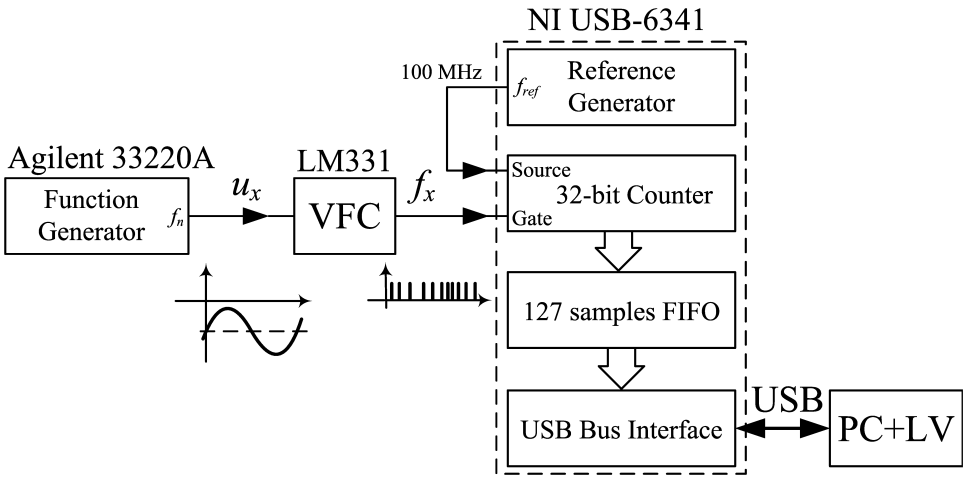

Fig. 7. Block diagram of the measuring circuit with weight averaging of pulse frequency signal.

The source of the test signal $u_x(t)$ was a programmable function generator Agilent 33220A [27]. The test signal was the sum of the DC component and the AC component:

$$u_x(t) = U_{DC} + U_m \cos(2\pi f_n t + \varphi_n)\ , \tag{64}$$

where: U_m is the amplitude of the test signal AC component, f_n is the frequency of the test signal, and φ_n is the initial phase of the test signal. Note that the sum of the DC component and the AC component must always be negative. The measurements of the output pulse signal of the VFC converter were carried out

using a pulse counter and the on-the-fly reading method. For this purpose, the NI USB-6341 measurement board [28] and a program written in LabVIEW environment were applied.

The system works as follows [29]. The function generator, programmed according to relation (64), generates a signal that is the sum of the component U_{DC} and harmonic distortion (3). The signal from the generator is passed to the input of the VFC converter, the output of which is a modulated pulse frequency signal $f_x(t)$ (63). The VFC output signal is then passed to the GATE input of the counter. The counter is configured to operate in the "Finite Buffered Edge Counting" mode [28]. In this mode, the 32-bit counter counts continuously the signal from the reference generator with frequency f_{ref} = 100 MHz [29].

The current contents of the counter generate a linear time scale with the resolution equal to the period of the reference signal $T_{ref} = 1 / f_{ref} = 10$ ns. Each time when applied to the counter's input GATE, the VFC output pulse snaps the current counter state into the FIFO register. The large capacity of the counter and the appropriately chosen reference frequency ensure that the counter overflow during the measurement. An overflow of the counter would occur only after 43 s of continuous operation. The program reads N_x counter states stored in the FIFO register and calculates the positions t_1, t_2, ..., t_{Nx} of the FVC output signal pulses, with the time distance between the first and last pulse having to be at least as large as the duration of the averaging window T, i.e., $t_{Nx} - t_1 >= T$ (Fig. 1).

Then the values of the weight function g_1, g_2, ..., g_{Nx} for times t_1, t_2, ..., t_{Nx} and the result of measurement of the VFC converter output frequency constant component f_0 are calculated (17). The measurement is repeated J times ($J = 100$) and the NMRR (5) is calculated, with the maximal value of error module $|\Delta|_{\max}(U_m)$ caused by interference of amplitude U_m calculated from the standard deviation of σ_{f0}:

$$\sigma_{f0} = \sqrt{\frac{1}{J-1}\sum_{j=1}^{J}\left(\overline{f_0} - f_{0j}\right)^2}, \tag{65}$$

where $\overline{f_0}$ is the average value of the J-series of the performed measurements, and f_{0j} is the j-th measurement result. Finally, the NMRR suppression coefficient of the signal data chain processed with weight averaging is calculated from the relation:

$$NMRR = 20\lg\left(\frac{S_f U_m}{\sqrt{2}\sigma_{f0}}\right), \tag{66}$$

where σ_{f0} is the standard deviation (65), U_{AC} is the amplitude of the test signal AC component, and $\sqrt{2}$ is the peak factor for the sinusoidal waveform.

Fig. 8 shows a complete block diagram of the test stand setup. In addition to the already discussed VFC converter, function generator, and counter, a Tektronix TDS210 digital oscilloscope and a PC2 were used to control the output voltage from the function generator and the pulsed output signal from the FVC. The function generator and the measuring card NI USB-6341 with counter were controlled via USB interface by the software realized in the LabVIEW environment installed on PC1.

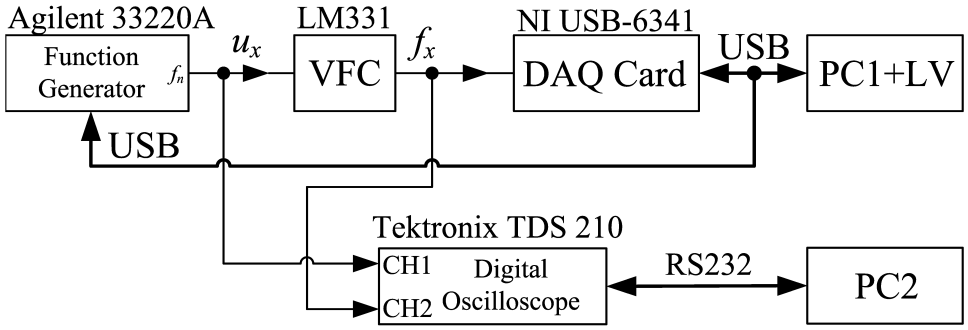

Fig. 8. Block diagram of the test stand for investigating weight averaging of pulse frequency modulated signal.

The actual appearance of the test stand is shown in Fig. 9. The use of two independently operating computers allows convenient control of correct operation of the apparatus and verification of the measurement algorithm.

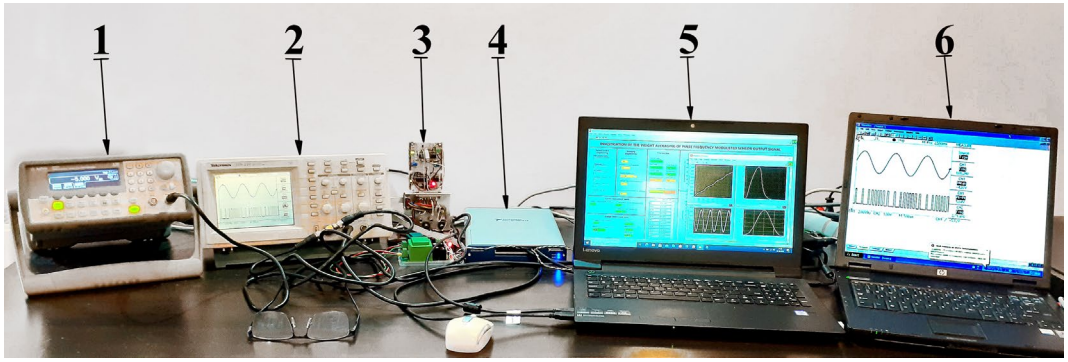

Fig. 9. Real view of the test stand for investigating weight averaging of pulse frequency modulated signal: 1 - function generator Agilent 33220A, 2 - digital oscilloscope Tektronix TDS210, 3 - voltage-to-frequency converter based on LM331 integrated circuit, 4 - Data Acquisition Card NI USB-6341, 5 - PC with LabVIEW software, 6 - PC for digital oscilloscope control.

Fig. 10 shows exemplary signals recorded during the tests.

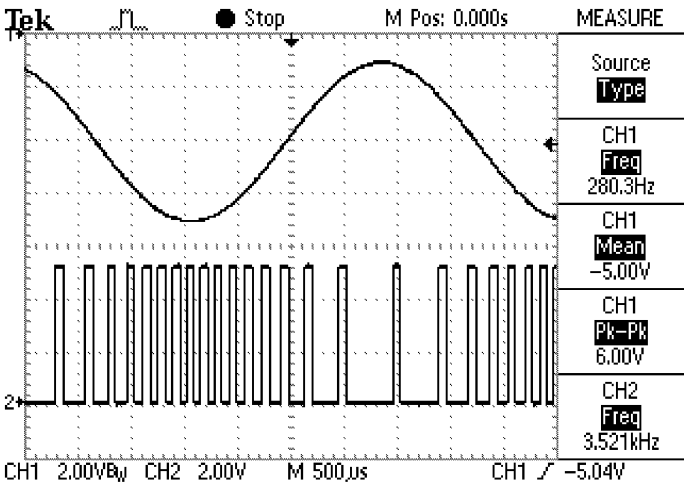

Fig. 10. Exemplary waveforms recorded during the test: top - output signal from functional generator Agilent 33220A, bottom - pulse output signal from voltage-to-frequency converter LM331.

In the first channel CH1, the DC component of the test signal U_{DC}= –5 V, the peak-to-peak value of the AC component 6 V = $2U_m$ (that is, the amplitude of the AC component U_m= 3 V), and the frequency of the test signal f_n = 280 Hz are measured, while in the CH2 channel, the output waveform from the VFC converter is observed. It can be noted that the oscilloscope has measured the value of the average frequency f_0 = 3.521 kHz, while the correct value determined by the weight averaging algorithm was 5 kHz.

5.2 Software control of measurements and data processing

Fig. 11 shows the block diagram of the algorithm that controls the operation of the test bench when weight averaging the frequency signal. The software was prepared in LabVIEW environment.

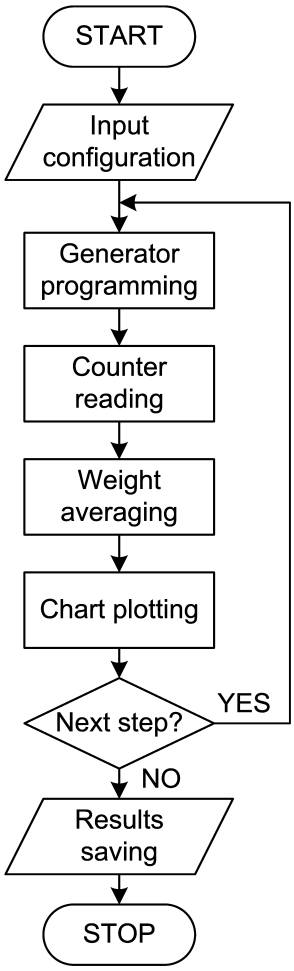

Fig. 11. Block diagram of the measuring algorithm for investigating weight averaging of pulse frequency modulated signal.

The sequence of tasks performed by the measurement algorithm is as follows:

1. Entering the input data into the algorithm:

(a) amplitude U_m of AC interference, and U_{DC} component of the signal,

b) initial frequency $f_{n\,min}$ of the interference, tuning step Δf_n of the function generator, and number of points of the suppression characteristic,

(c) sensitivity S_f of the VFC converter,

(d) type and duration T of the weight function $g(t)$,

(e) number J of repeated measurements for each value of interference frequency f_n;

2. For a fixed value of interference frequency f_n, making a counter measurement of times t_1, t_2, ... t_i, ..., t_{Nx}, for successive pulses of the VFC output signal;

3. Calculating the values $g_i=g(t_i)$ of the weight function (Fig. 1) and summing them (17) to obtain the value of the weight averaged VFC output frequency f_0;

4. Repeating J times the points 2, 3 and calculating NMRR (66);

5. Increasing the interference frequency f_n by step Δf_n and repeating steps 2, 3, and 4 until the maximum value $f_{n\,max}$ is reached;

5. Repeating steps 2, 3, 4,… for each successive value of interference frequency f_n;

6. Plotting the characteristics of NMRR as a function of frequency f_n, saving the results to a file, and comparing with the theoretical characteristics.

It should be noted that the frequency signal has a peculiar property which manifests itself in the fact that for the same periodically repeated values of the VFC converter input signal, different positions of pulses in successive periods of interference are obtained, i.e., a different sequence of times t_i at which the

VFC output pulses appear. Therefore, for each successive value of the disturbance frequency f_n, a series of measurements must be made and the results averaged to determine the NMRR.

The most important part of the presented algorithm is weight averaging of the frequency signal. Fig. 12 shows an exemplary diagram of the averaging algorithm with the Blackman-Harris weight function. The algorithm calculates the values $g_i=g(t_i)$ of the weight function according to relation (54) based on the values of the measured times t_i contained in the Pulse time [s] matrix. The weight averaged measurement result is calculated by summing up all g_i coefficients. Fig. 13 shows the control panel of the virtual instrument realized in the LabVIEW environment for the presented research.

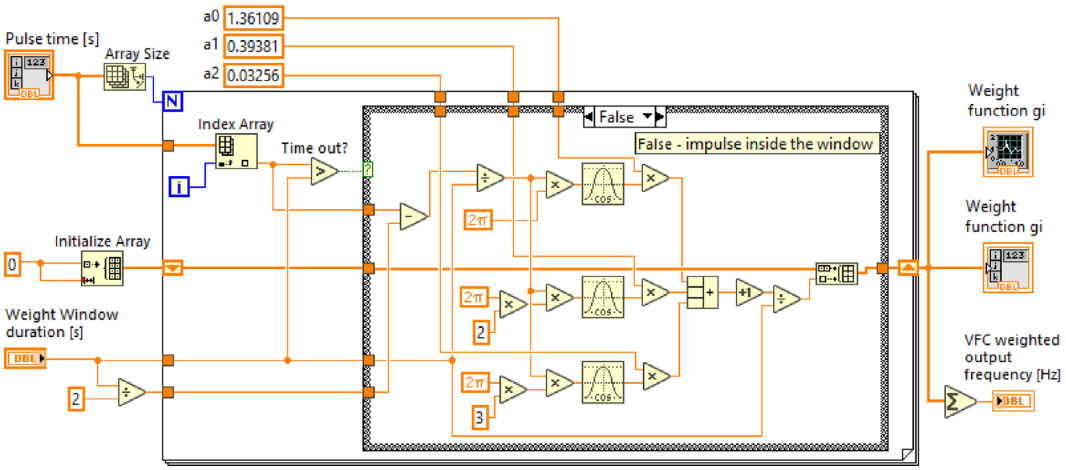

Fig. 12. Exemplary LabVIEW diagram for Blackman-Harris weight averaging (54).

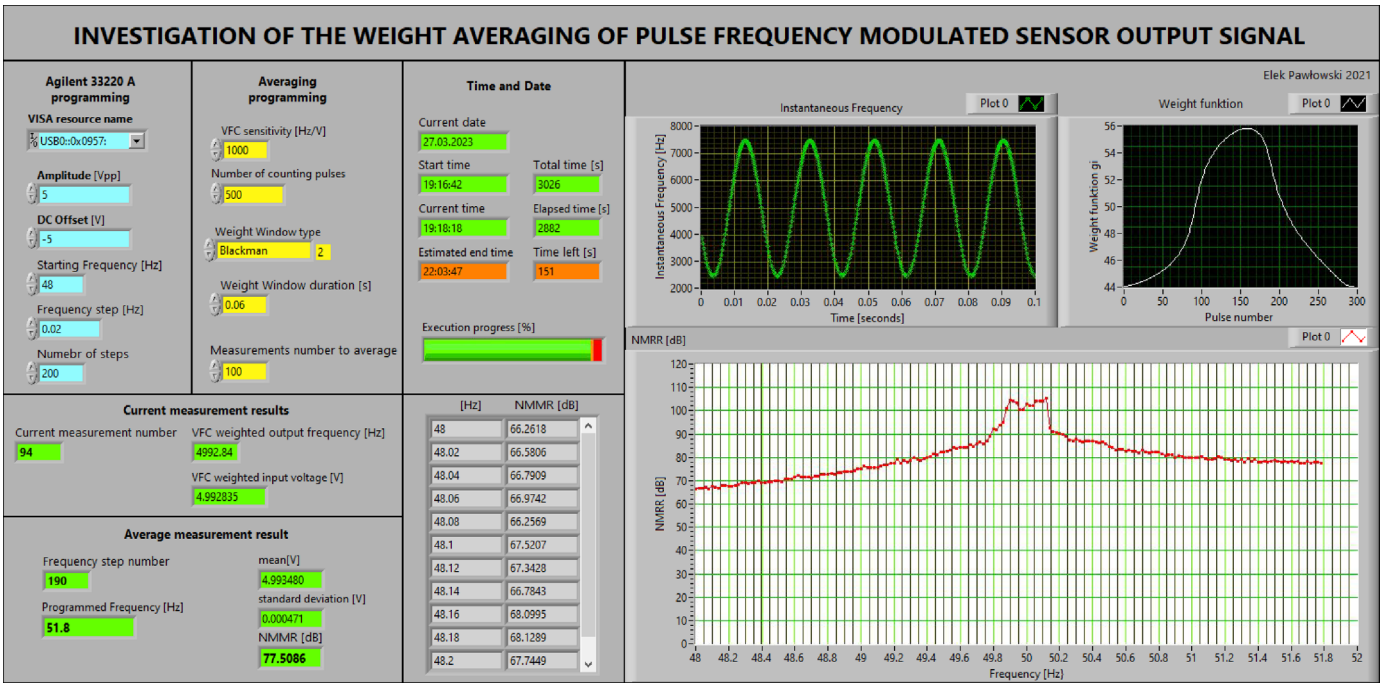

Fig. 13. Panel of the virtual instrument for investigating of weight averaging of pulse modulated frequency.

5.3 Results of measurement

Three series of measurements were performed: (1) over a wide frequency range from 2 Hz to 1000 Hz with step of 2 Hz, at constant amplitude U_m and constant DC component U_{DC}, (2) over a narrow frequency range from 48 Hz to 52 Hz with step of 0.02 Hz, at constant U_m and U_{DC}, and (3) for different values of U_m and U_{DC} falling within the VFC processing range. A selection of most representative

measurement results is discussed in the paper, while all realized measurements are available in the repository [26].

5.3.1. Measurement results over wide frequency range from 2 Hz to 1000 Hz

In the wide frequency range from 2 Hz to 1000 Hz, four series of measurements were performed with step of 2 Hz (500 points), at constant amplitude $U_m = 2.5$ V and constant DC component $U_{DC} = -5$ V. The amplitude and DC component were selected so that the test signal was between 25% and 75% of the full measurement range of the VFC converter. Each series of measurement was carried out for a different averaging window with appropriately selected averaging time: uniform (rectangular) window, time 20 ms, triangular window, time 40 ms, Blackman window, time 60 ms, and Blackman-Harris window, time 80 ms. Each measurement point on the graph was calculated by averaging 100 measurements, which took about 15 seconds. Calculating one complete series of measurements of 500 points took about 2 hours. The resulting NMRR values are shown in Fig. 14.

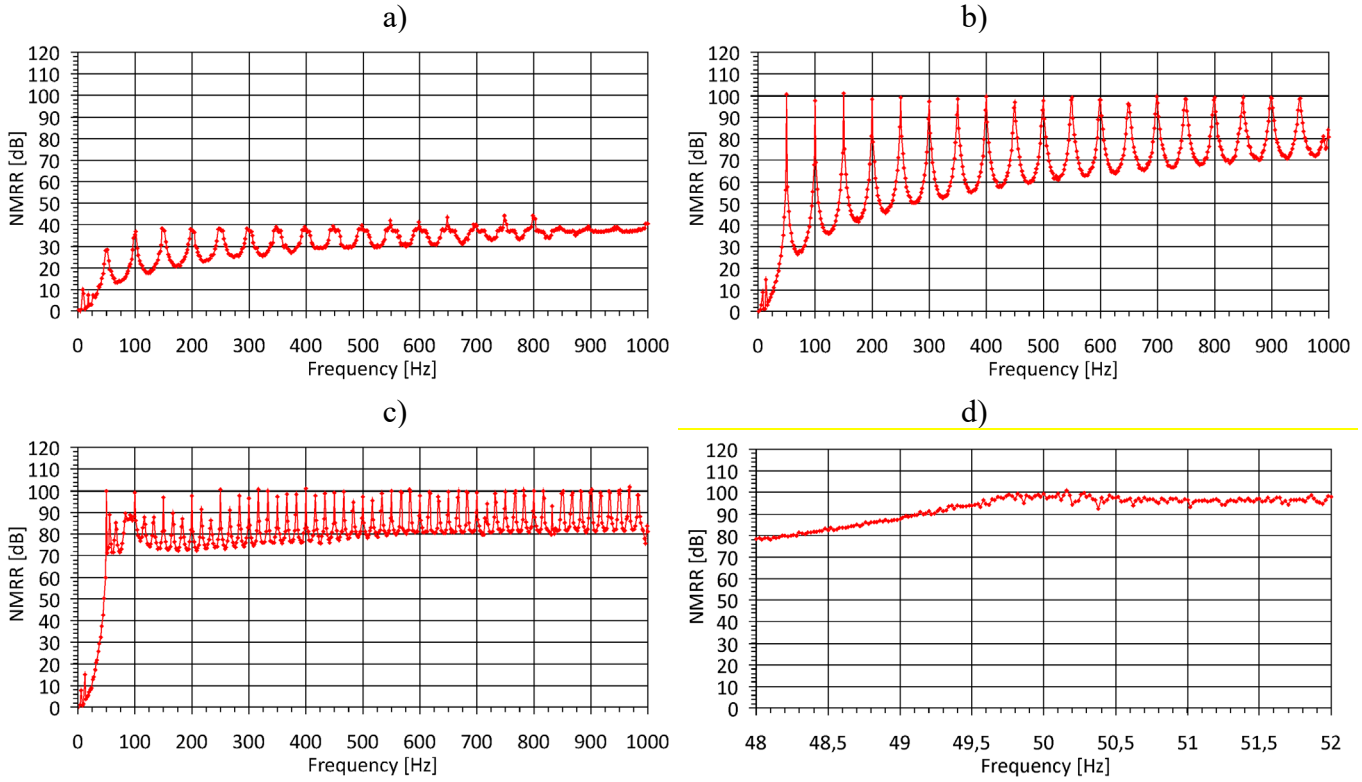

Fig. 14. NMRR as function of interference frequency - measurements in the range of 2 Hz-1000 Hz, step 2 Hz (500 points), amplitude $U_m = 2.5$ V, DC component $U_{DC} = -5$ V: a) uniform (rectangular) window, time 20 ms, b) triangular window, time 40 ms, c) Blackman window, time 60 ms, d) Blackman-Harris window, time 80 ms.

When analyzing the results presented in Fig. 14, good agreement with the results of the theoretical analysis and the earlier presented simulations is observed. However, some differences are also visible. In Fig. 14a for the uniform (rectangular) window, large suppression can be observed for the frequency close to 50 Hz and its integer multiples. This effect can be explained by the large value of the quantization error for the uniform (rectangular) window, which makes it impossible to observe small frequency changes, an effect similar to the large value of NMRR.

5.3.2. Measurements in short frequency range near 50 Hz

In the short frequency range from 48 Hz to 52 Hz, four series of measurements were made with step of 0.02 Hz (201 points). The other parameters of the measurements were assumed the same as in the

previous part: amplitude $U_m = 2.5$ V, and DC component $U_{DC} = -5$ V. Each series of measurements was carried out for a different averaging window with appropriately selected averaging time: uniform (rectangular) window, time 20 ms, triangular window, time 40 ms, Blackman window, time 60 ms, and Blackman-Harris window, time 80 ms. Each measurement point on the graph was calculated by averaging 100 measurements, which took about 15 seconds. Calculating one complete series of measurements of 200 points took about 50 minutes. The obtained NMRR values are shown in Fig. 15.

When analyzing the results presented in Fig. 15, good consistency with the results of the theoretical analysis and the earlier presented simulations is also observed. However, some differences are also visible near the frequency of 50 Hz. In Fig. 15a for the uniform (rectangular) window, one can see large NMRR values (off-chart, about 300 dB) in the ±0.1 Hz range around 50 Hz. Fig. 15c for the Blackman window in the ±0.1 Hz range around 50 Hz shows a pronounced flattening. A similar effect, but to a lesser extent, is noticed for the triangular and Blackman-Harris windows.

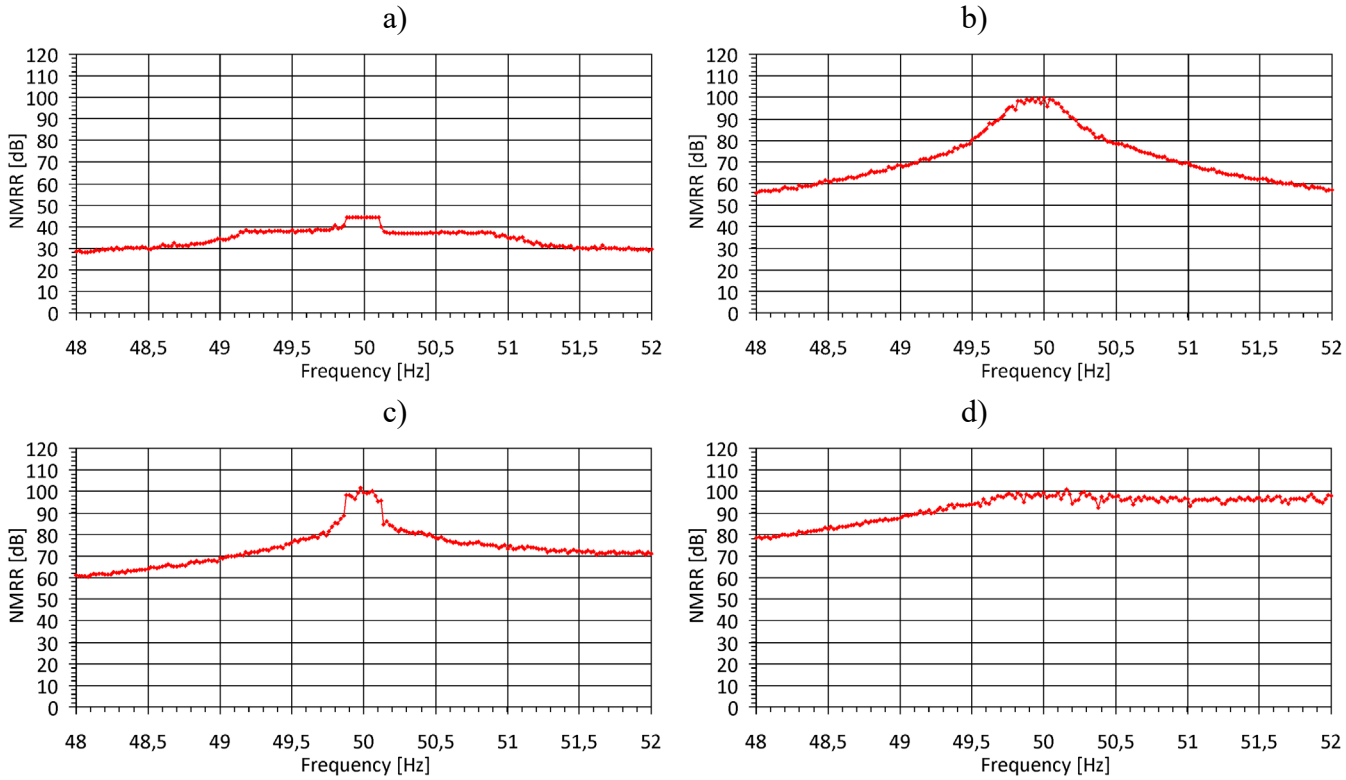

Fig. 15. NMRR as function of interference frequency - measurements in the range of 48 Hz-52 Hz, step 0.02 Hz (201 points), amplitude $U_m = 2.5$ V, DC component $U_{DC} = -5$ V: (a) uniform (rectangular) window, time 20 ms, (b) triangular window, time 40 ms, (c) Blackman window, time 60 ms, (d) Blackman-Harris window, time 80 ms.

5.3.3. Measurement results for different values of amplitude and DC component

In the next step, the effect of the DC component U_{DC} and the amplitude U_m on the NMRR was investigated. The measurements were made for the Blackman window with an averaging time of 60 ms. In the frequency range of 48 Hz – 52 Hz with step of 0.02 Hz (201 points), three series of measurements were made for DC component $U_{DC} = -5$ V and different amplitudes: $U_m = 1$ V, 2.5 V, 4.5 V, followed by three measurement series for amplitude $U_m = 2.5$ V and different values of DC component: $U_{DC} = -3$ V, –5 V, –7 V. Each measurement point on the graph was calculated by averaging 100 measurements. The obtained values of NMRR are shown in Fig. 16.

When analyzing the results presented in Fig. 16, it can be seen that the suppression characteristics are more influenced by the amplitude U_m, while the DC component U_{DC} is less important. For the smallest amplitude $U_m = 1$ V, (Fig. 16a), the graph shows a pronounced flattening at 90 dB in the frequency range of ±0.4 Hz around 50 Hz, while for the largest amplitude, $U_m = 4.5$ V, (Fig. 16c), a pronounced flattening

is observed at over 100 dB in the ±0.4 Hz frequency range around 50 Hz. In contrast, Fig. 16e, f, g for amplitude U_{AC} = 2.5 V and different values of component U_{DC} show no significant differences. Thus, it can be concluded that weight averaging is more effective for larger AC components of the test signal.

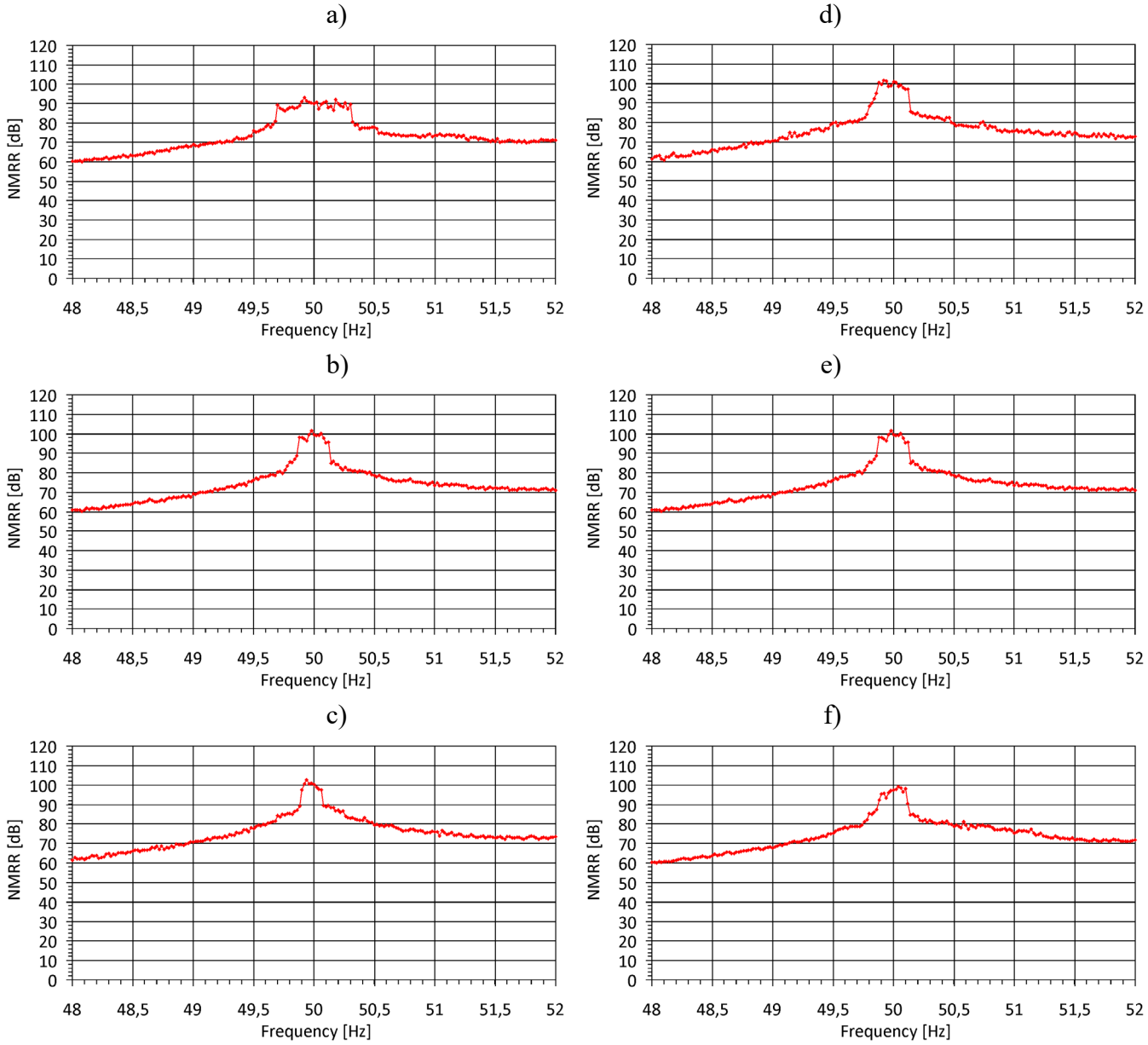

Fig. 16. NMRR as function of interference frequency - measurements in the range 48 Hz-52 Hz, step 0.02 Hz (201 points), Blackman averaging window, time 60 ms. On the left (a, b, c) - value of DC component U_{DC} = –5 V: a) U_m = 1 V, b) U_m = 2.5 V, c) U_m = 4.5V, on the right (d, e, f) - amplitude U_m = 2.5 V: d) U_{DC} = –3 V, e) U_{DC} = –5 V, f) U_{DC} = –7 V.

5.4 Discussion of the obtained experimental results

Summary plots were made to summarize the obtained experimental results. Fig. 17 shows a comparison of NMRR as a function of interference frequency for four windows with appropriately selected averaging times: uniform (rectangular) window, time 20 ms, triangular window, time 40 ms, Blackman window, time 60 ms, and Blackman-Harris window, time 80 ms. The measurements were performed in the range of 2 Hz - 1000 Hz with step 2 Hz (500 points), at amplitude U_m = 2.5 V and DC component U_{DC} = –5 V.

The measurement results shown in Fig. 17 confirm the theoretical relationships that the worst performance is for the rectangular window, for which the NMRR reaches values of only 40 dB. For the

other windows, triangular, Blackman, and Blackman-Harris (with appropriately chosen averaging times), the maximum values of NMRR are close to 100 dB. However, the triangular window shows a large variation in NMRR from 30 dB to 100 dB, while for the Blackman window this variation is from 70 dB to 100 dB, and for the Blackman-Harris window only from 95 dB to 100 dB. Thus, the experiments confirmed very good theoretical properties of the Blackman and Blackman-Harris windows. It should also be taken into account that a longer measurement window means more pulses for which the g_i coefficients of the averaging window are calculated (42), (45), (51), (54), which means a more accurate realization of the theoretical window shape.

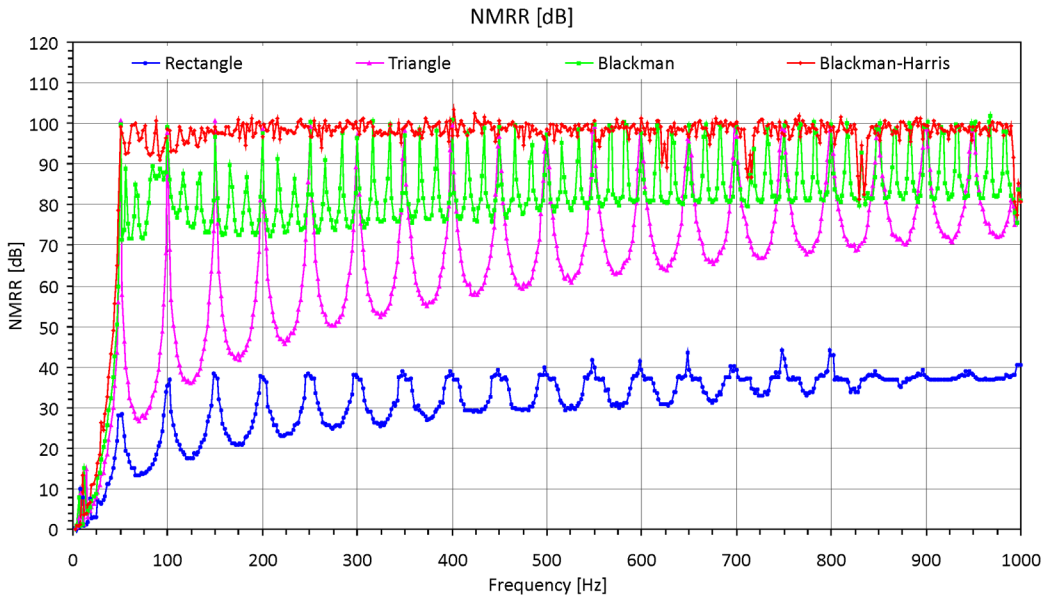

Fig. 17. Comparison of NMRR as function of interference frequency for different windows: uniform (rectangular), time 20 ms, triangular, time 40 ms, Blackman, time 60 ms, Blackman-Harris, time 80 ms - measurements in the range of 2 Hz – 1000 Hz, step 2 Hz (500 points), amplitude $U_m = 2.5$ V, DC component $U_{DC} = -5$ V.

Fig. 18 shows a comparison of NMRR for four averaging windows as a function of interference frequency over a narrow frequency range of 48 Hz - 52 Hz with step of 0.02 Hz (201 points), amplitude $U_m = 2.5$ V, and component $U_{DC} = -5$ V. For the Blackman and Blackman-Harris windows, the averaging time was 60 ms and 80 ms, respectively. For the rectangular window, the measurements were made with an averaging time of 20 ms and an additional time of 80 ms. For the triangular window, the measurements were made with an averaging time of 40 ms and 80 ms. The additional measurements, with the averaging time increasing to 80 ms for the uniform (rectangular) and triangular windows, were made to compare with the Blackman-Harris 80 ms window.

The measurement results presented in Fig. 18 clearly show that the maximum NMRR for the triangular, Blackman, Blackman-Harris windows has a similar value of 100 dB. However, the triangular window shows much worse suppression for frequencies different from 50 Hz. The Blackman-Harris window, which is the best in this respect, shows the least variation in the suppression of about 5 dB for frequencies greater than 50 Hz.

Additional measurements made with an averaging time of 80 ms for the rectangular and triangular windows have shown that simply extending the averaging time for these windows does not give as good results as the Blackman-Harris 80ms weight function. Extending the uniform (rectangular) window from 20 ms to 80 ms increased the NMRR from 38 dB to only 50 dB, while the Blackman-Harris 80 ms window has a suppression of 100 dB. An analogous lengthening of the triangular window from 20 ms to 80 ms produced virtually no noticeable increase in NMRR.

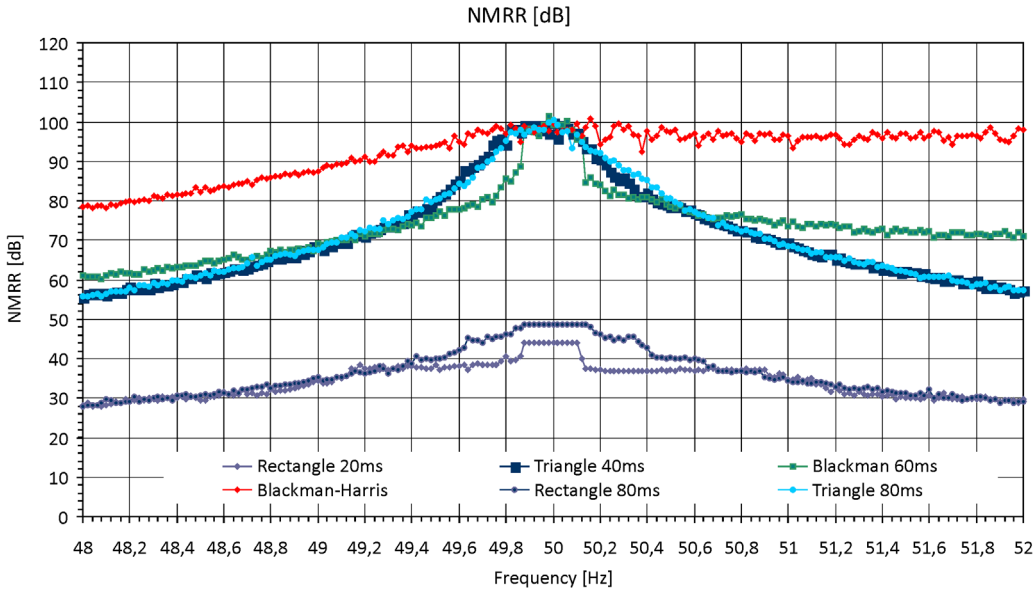

Fig. 18. Comparison of NMRR as function of interference frequency for different windows: uniform (rectangular), time 20 ms, 80 ms, triangular, time 40 ms, 80 ms, Blackman, time 60 ms, Blackman-Harris, time 80 ms, - measurements in the range of 48 Hz - 52 Hz, step 0.02 Hz (201 points), amplitude $U_m = 2.5$ V, $U_{DC} = -5$ V.

Fig. 19 shows a comparison of NMRR for the Blackman window with averaging time of 60 ms, as a function of interference frequency over a narrow frequency range of 49.4 Hz - 50.6 Hz with step of 0.02 Hz. The effect of the DC component and amplitude on the NMRR suppression ratio was studied. The measurements were made for amplitudes: $U_m = 1$ V, 2.5 V, 4.5 V, and DC component values: $U_{DC} = -2$ V, –3 V, –5 V, –7 V, –9 V. Only those combinations of constant component and amplitude whose sum fell within the VFC processing range were considered.

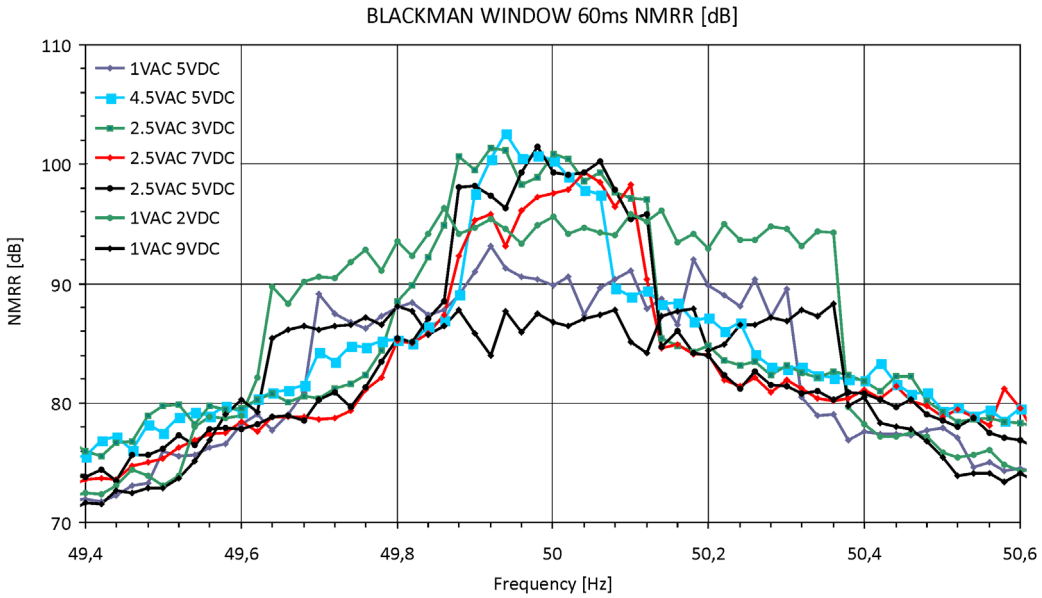

Fig. 19. NMRR as function of interference frequency - measurements in the range 49.4 Hz - 50.6 Hz, step 0.02 Hz, Blackman averaging window, time 60 ms, amplitudes: $U_m = 1$ V, 2.5 V, 4.5 V, DC component values: $U_{DC} = -2$ V, –3 V, –5 V, –7 V, –9 V.

The measurement results shown in Fig. 19 clearly show that the values of amplitude U_m and DC component U_{DC} of the test signal significantly affect the suppression near 50 Hz, where the observed changes in NMRR were about 15 dB. For frequencies differing from 50 Hz by more than ±0.5 Hz, the suppression changes are smaller, about 5 dB. The graph also shows that the maximum suppression value is

more influenced by the amplitude U_m, i.e., the larger the amplitude, the greater the suppression. On the other hand, the DC component has more influence on the width of the peak of the NMRR, especially for small amplitudes U_m. In this case, a larger DC component (as to modulus) results in a wider peak. For the smallest amplitude U_m =1 V and the largest DC component U_{DC} = –9 V, the graph shows a pronounced flattening at 85 dB in the frequency range of ±0.4 Hz around 50 Hz, while for the largest amplitude U_m= 4.5 V and the DC component U_{DC} = –5 V, a pronounced flattening is observed at the level of more than 100 dB in the frequency interval of ±0.1 Hz around 50 Hz. Thus, it can be concluded that weight averaging is more effective for larger AC components of the test signal.

6. Conclusions

The uncertainty of measurement of the VFC output pulse frequency contains two main components, which are caused by: i) counting the impulses in the given time interval and ii) the influence of the interference in the VFC input signal. The output frequency weight averaging with an appropriately selected weight function (window) provides two positive features: i) reduction of the pulse counting effect, and ii) suppression of periodical harmonic components of the interference at a given level in a narrow or wide frequency band. The result of the VFC output frequency measurement is the sum of values of the weight function samples taken at the time of appearance of VFC output pulses.

Using weight averaging to measure of VFC output frequency, the effect of pulse counting is transformed into the effects associated with sampling the weight function. Therefore, this component of uncertainty depends on the shape of the weight function and the number of pulses placed in the function's durability. When the so-called polynomial weight functions, i.e. triangular, parabolic, etc., are used, the relative error, caused by sampling, decreases proportionally to the corresponding power of the number of pulses N_x in the duration of the function, namely, for triangular functions this decrease is proportional to N_x^2, and for parabolic it is proportional to N_x^3, etc. Such weight functions at the same time provide an increase in the level of suppression (NMRR) of periodic interference with a relatively stable frequency (relative instability is about a few %). However, the level of side lobe of the spectral characteristics of these functions is relatively high: about -27 dB for the triangular and -40 dB for the parabolic function, therefore such functions are not effective for suppressing interference whose frequency can vary over a wide bandwidth. Besides, with the increase in the order of the polynomial function (window) requires a corresponding increase in the averaging time of the frequency measurement in the presence of interference, namely 2 times for the triangular function and 3 times for the parabolic function.

The effective suppression interferences with unstable frequency and even in the absence of knowledge of the interference frequency values in the preset range, can be obtained by the weight functions with appropriate low level of side lobes of the spectral characteristic. The use of the Blackman weight function, which duration is equal to 3 periods of least-frequency interference, ensures suppression (NMRR) of periodic interferences at a minimum level of 70 dB, while the counting effect is reduced to a level about 90 times lower than the usual pulse counting. To increase the NMRR and reduce the counting effect, other weight functions can be used, for example the Blackman-Harris function with duration of 4 periods of least-frequency interference provides NMRR over 90 dB and reduction of counting effect about 5800 times.

Simulation tests of weight averaging by the uniform (rectangular), triangular, Blackman and Blackman-Harris weight functions for averaging time of 60 ms give the values of the counting error component which are very close to the theoretical values. Simulation tests of suppression of periodic interferences in a narrow frequency band, ±2% from nominal frequency 50 Hz, for the worst phase of interference, have shown that using the triangular window (averaging time 40 ms) and Blackman window (averaging time 60 ms) also gives the values of NMRR very close to the theoretical ones. Results of simulation shows that using the Blackman window the values of NMRR for any frequency above the minimum value $f_{\min} = 3/T$ (T is function duration) are very close to the theoretical levels. That means that

the performed simulations fully confirm the previously obtained theoretical results regarding the both components: counting effects and NMRR of input voltage interference during weight averaging of VFC output pulses.

When, caused by random noise in the input signal and in the elements of the VFC chain, the standard deviation of the temporal variances of the pulses does not exceed 0.5 - 2% of the pulses period, the influence of these factors on the averaging result is relatively small.

The presented and discussed above results of extensive experimental study of weight averaging of VFC output frequency pulses at different values of input voltage and parameters of interference have shown very good consistence with the results of the simulation studies and the theory.

Detailed results obtained in the process of simulation and experimental studies are given in [30] and [31], respectively.

Literature:

1. Walt Kester (2004), *Analog-Digital Conversion*, Analog Devices, 2004, ISBN 0-916550-27-3, Chapter 3.
2. *The Data Conversion Handbook*, Elsevier/Newnes (2005), ISBN 0-7506-7841-0, Chapter 3.
3. John L. Lindesmith, "Voltage-to-Digital Measuring Circuit," *U.S. Patent 2,835,868*, filed September 16, 1952, issued May 20, 1958.
4. Paul Klonowski, "Analog-to-Digital Conversion Using Voltage-to-Frequency Converters," *Application Note AN-276*, Analog Devices, Inc.
5. James M. Bryant, "Voltage-to-Frequency Converters," *Application Note AN-361*, Analog Devices, Inc.
6. Steve Martin, "Using the AD650 Voltage-to-Frequency Converter as a Frequency-to-Voltage Converter," *Application Note AN-279*, Analog Devices, Inc.
7. High-Frequency Voltage-to-Frequency Converter, VFC110, Texas Instruments, Dallas 2022.
8. D. McDonagh, K. I. Arshak (1998), Stable Differential Voltage to Frequency Converter with Low Supply Voltage and Frequency Offset Control, IEEE Transactions on Instrumentation and Measurements, vol. 47, No 5, October 1998, s. 1355-1361.
9. F. N. Trofimenkoff, F. Sabouri, J. Qin, J. W. Haslett (1997), A Square-Rooting Voltage-to-Frequency Converter, IEEE Transactions on Instrumentation and Measurements, vol. 46, No 5, October 1997, s. 1208-1211.
10. E. Pawlowski (2017), Design and evaluation of a flow-to-frequency converter circuit with thermal feedback, IOP Publishing Ltd, Measurement Science and Technology, vol. 28, pp. 054004, May 2017.
11. Świsulski, D., Pawłowski, E., Dorozhovets M. (2018), Digital processing of frequency–pulse signal in measurement system. Lecture Notes in Electrical Engineering. Volume 452, 2018, pages 319-332.
12. D. Arbet, M. Kováč, V. Stopjaková and M. Potočný, "Voltage-to-Frequency Converter for Ultra-Low-Voltage Applications," *2019 42nd International Convention on Information and Communication Technology, Electronics and Microelectronics (MIPRO)*, Opatija, Croatia, 2019, pp. 53-58, doi: 10.23919/MIPRO.2019.8756910.
13. Y. Xu *et al*., "An Integrator and Schmitt Trigger Based Voltage-to-Frequency Converter Using Unipolar Metal-Oxide Thin Film Transistors," in *IEEE Journal of the Electron Devices Society*, vol. 9, pp. 144-150, 2021, doi: 10.1109/JEDS.2020.3045160.
14. Jongha Park, Jung-Hyun Park and Seong-Ook Jung Current Measurement Transducer Based on Current-To-Voltage-To-Frequency Converting Ring Oscillator with Cascade Bias Circuit. *Sensors* 2020, *20*(2), 493; https://doi.org/10.3390/s20020493.
15. A. Von Hoegen, G. Götz, N. Hartgenbusch, R. W. De Doncker and T. Kojima, "Precise Volt-Second Measuring Instrument for Voltage-Source Inverters," *2022 25th International Conference on Electrical Machines and Systems (ICEMS)*, Chiang Mai, Thailand, 2022, pp. 1-6, doi: 10.1109/ICEMS56177.2022.9982988.
16. C. C. Wang, Z. -Y. Hou and J. -C. You, Temperature-to-Frequency Converter With 1.47% Error Using Thermistor Linearity Calibration, in *IEEE Sensors Journal*, vol. 19, no. 13, pp. 4804-4811, 1 July1, 2019, doi: 10.1109/JSEN.2019.2903713.
17. B. N. Mohapatra, J. Joshi, A. Wathe, A. Chanakhekar, A. Patil, V. Phadtare. Simulation design performance for power supply and a variable voltage to frequency converter. Journal of Engineering Sciences. Vol. XXVII, no. 4 (2020), pp. 76 - 79, DOI: https://doi.org/10.5281/zenodo.4288269.
18. Asna, M., Shareef, H., Khalid, S. N., Al Dosari, A., Hamad, B., Alhammadi, M., & Aldarmaki, N. (2019). Analysis and design of single phase voltage-frequency converter with optimized PI controller. *International Journal of Power Electronics and Drive Systems*, *10*(1), 522-529. https://doi.org/10.11591/ijpeds.v10n1.pp522-529.
19. Zelin Li and Gaofeng Pan, Design of real time system to measure the voltage signal in high voltage power supply, Journal of Physics: Conference Series 1887 (2021) 012023 IOP Publishing doi:10.1088/1742-6596/1887/1/012023.
20. EN 50160, Voltage characteristics of electricity supplied by public distribution systems, 1999.

21. J. Mindykowski, T. Tarasiuk, E. Szmit, D. Czarkowski (2006), Diagnostyka izolowanego systemu elektroenergetycznego na przykładzie jednostki pływającej (Diagnostics of isolated electrical power system on example of the ship). DIAGNOSTYKA'2 (38)/2006. (In Polish).
22. Dorozhovets M. (1985), Modulacionnyje metody viesovogo usrienienia. (Modulation weight averaging methods). Izvestia Vyzhshikh Uchebnykh Zaviedienij. Priborostrojenie. T. XXVIII, N3, LITMO, 1985. (In Russian).
23. Poularikas A. D. (1999), Windows. *The Handbook of Formulas and Tables for Signal Processing.* Ed. Alexander D. Poularikas, Boca Raton: CRC Press LLC, 1999.
24. G. A. Korn, Th. M. Korn (1968), Mathematical Handbook For Scientists And Engineers, 1968.
25. Berezin L.V., Vejtsel V.A. (1977), Teoria i projektirovanije radiosistem. (Theory and design of radio systems). Pod. Red. V.N.Tipugina. M.: Sov. Radio, 1977, 448 s. (In Russian).
26. LMx31x Precision Voltage-to-Frequency Converters, Data sheet, SNOSBI2C –JUNE 1999–REVISED SEPTEMBER 2015, Texas Instruments Incorporated.
27. Agilent 33220A 20 MHz Function /Arbitrary Waveform Generator, User's Guide, Agilent Technologies, Publication Number 33220-90002 Edition 4, May 2007, Agilent Technologies, Inc.
28. DAQ X Series NI 632x/634x/635x/636x Devices, User Manual, August 2010, 370784B-01, National Instruments Corporation.
29. Pawlowski E. (2014), Digital processing of pulse signal from light-to-frequency converter under dynamic condition, Proc. SPIE 9291, 13th International Scientific Conference on Optical Sensors and Electronic Sensors, 19 August 2014, 929102, doi.org/10.1117/12.2065028.
30. Dorozhovets, M., Pawłowski, E., Świsulski, D. (2022). *Simulation of the weight averaging of pulse frequency modulated sensor output signal* [Data set]. Gdańsk University of Technology. https://doi.org/10.34808/vbsc-7z61.
31. Pawłowski, E., Świsulski, D., Dorozhovets, M. (2022). *Experimental investigation of the weight averaging of pulse frequency modulated sensor output signal* [Data set]. Gdańsk University of Technology. https://doi.org/10.34808/79d9-pt39.